Chapter 2

Additively Manufacturing Metal−Organic Frameworks and Derivatives: Methods, Functional Objects, and Applications

Desheng Liu,[1,2] Pan Jiang,[1,2] Xiaolong Wang,[*,1,2] and Weimin Liu[*,1]

[1]State Key Laboratory of Solid Lubrication, Lanzhou Institute of Chemical Physics, Chinese Academy of Sciences, Lanzhou 730000, China

[2]Center of Materials Science and Optoelectronics Engineering, University of Chinese Academy of Sciences, Beijing 100049, China

[*]Email: wangxl@licp.cas.cn (X. Wang)

[*]Email: wmliu@licp.cas.cn (W. Liu)

Metal-organic frameworks (MOFs) are emerging porous crystalline materials that are composed of inorganic building units self-assembled with organic linkers. They have been intensively investigated because of their high porosity and designable functionality. However, one of the biggest drawbacks of MOF crystals is its large-scale application, primarily due to the rigid and brittle powder forms, as well as the low chemical stability and limited mechanical properties. Hence, the fabrication of MOF-based monolithic materials with easy recovery and tailorable shapes has become a fundamental challeng. To address, powdery MOFs need to be processed into structured monoliths with exceptional performance in well-defined and customizable forms. Additive manufacturing (AM), usually known as three-dimensional (3D) printing, has been considered as a potential strategy for manufacturing MOF-based structural and functional devices, where their properties can be regulated by the structure design to meet the practical application. Up to date, several 3D printing technologies such as fused deposition modeling, powder-based selective laser sintering, direct ink writing and digital light processing have been employed to engineer the customizable MOF components. Various 3D printed MOF structures and devices have been intensively investigated in various applications, such as 3D light-emitting objects with various shapes, 3D flow-through filters for capturing toxic gases, 3D scaffolds with drug delivery and bone regeneration, and 3D porous monolithic catalytic devices for water purification. Therefore, it is possible to construct MOF-based devices with desirable structures by combining 3D printing with MOF crystals to provide potentially industry-available commodities closely related with chemicals, environment, and energy.

Ghosh et al.; MetalOrganic Frameworks for Carbon Capture and Energy
ACS Symposium Series; American Chemical Society: Washington, DC, 2021.

Introduction

Metal-organic frameworks (MOFs) are an emerging class of crystalline porous materials that are composed of inorganic metal cations coordinated with organic linking ligands (*1*). The unique features of MOFs lie in uniformly arranged open channels or cavities, predictable pore size, large internal surface areas and porosities, and tailorable chemical components and architectures, thereby offering enormous potential in many applications including catalysis (*2*), gas storage and separation (*3*), drug delivery (*4*), wastewater treatment (*5*), biomedical imaging and sensing (*6*). However, MOFs crystalline powders are generally brittle in nature, and MOFs powder can also cause some issues like difficult collection and secondary pollution, resulting in severe restrictions on the wide spread industrial applications of MOFs. For successfully large-scale applications and commercialization, MOFs must be formulated into bulk structures with desirable properties, such as extremely high porosity and accessible surface area. Unfortunately, due to the lack of thermoplasticity, the processability and handling of MOFs is remarkably low. A mitigation strategy is integrating MOF particles with polymer composites to improve their processabilities, thereby further expanding their applications (*7*, *8*).

To achieve this, a huge range of MOFs have been pelletized to form pellets or granules (*9*, *10*), or incorporated with polymer matrix to be shaped into other structures with good flexibility and large permeability, such as films, membranes, filaments, spheres, and so on (*11*, *12*). However, these bulk materials generally reduce the functionality of the resultant MOFs monolith structures, such as blocking the accessible pores and reducing the surface area of MOFs, limiting the mass transfer, and meanwhile the mechanical force from the processing process damages the crystallinity of MOFs. Besides, the MOFs can also be anchored onto the various shaped supports to fabricate the multifunctional devices used in different applications, such as drug release, wastewater treatment, and gas separation (*13*–*15*). Although this strategy does not destroy the unique crystallinity of MOFs, it reduces the loading of MOFs and causes the material loss and device contamination at high flow rates. That being stated, the bulk MOFs materials achieved by traditional shaping and densification approaches are generally unsuitable for large-scale industrial applications. Most applications would benefit if the combination of MOFs powder with 3D printing technologies to fabricate multiscale functional structured MOFs with adjustable porous architectures.

Compared with traditional fabrication processes, the emerging 3D printing technology can be utilized to manufacture many functional parts and devices that possess complex structural construction, tunable chemical properties, and excellent regeneration and reuse potential (*16*, *17*). Employing 3D printing technique can shape porous MOFs material into structured components or devices, including adsorbents (*18*), filters (*19*), membranes (*20*), and catalytic reactors for water purification (*21*). In addition, 3D printing dispalys the advantage of fine-tuning the microstructure of the printed objects, which allows to construct the intricate structures with functional surfaces. In recent years, the common 3D printing technologies used to manufacture 3D MOF-polymer composites include direct ink writing (DIW) (*22*), fused deposition modeling (FDM) (*23*), digital light processing (DLP) or stereolithography (SLA) (*24*), and selective laser sintering (SLS) (*25*). In most cases, there are two strategies to achieve the 3D printed MOF structures with complex geometries, controlled pore structure and porosity, and up-scalability. The first and also the more challenging one is to directly print MOFs into 3D complex structures by mixing MOF particles into polymer solution or 3D printable mixture (*26*). The alternative is the surface modification, often based on *in situ* growing MOFs layer-by-layer on the surface of 3D printed devices or cellular supports, or inside the 3D printed polymer support. Hence, the latter design based on 3D printing

skeleton surface functionalization provides the significant advantage over the integrated manufacturing of 3D MOFs materials.

In this chapter, we summarize the recent progress in the preparation of 3D printed robust macroscale MOFs materials by combining MOFs with various 3D printing technologies. The 3D printed MOFs structures with customized shapes can meet the requirements from different applications, including water treatment, catalysis, gas and energy storage, gas adsorption, moisture sensing, optics, and bioengineering. For 3D MOF-based composites prepared by FDM 3D printing, they usually had the limitations of low MOFs loading, poor porosity, and relatively rigid and brittle polymer matrices. The DIW methods for 3D printing of MOF-contained composites generally prepared the MOF-based printable inks by directly blending MOFs into polymer precurosor (*i.e.,* rheology modifiers and plasticizers). Unfortunately, the approach embeded the MOFs into the polymer matrix material, resulting in the block of the porous properties of the MOFs, thereby reducing the comprehenssive performance. In the case of DLP or SLA 3D printing, the MOFs crystals were dispersed into the photopolymerizable resins, which can be used to achieve the porous and flexible 3D MOFs structures by the spatially controlled polymerization curing step. While the main drawback is that the a significant quantity of polymers can shade the role of MOFs. The pre-synthesized MOFs fillers and polymer particles were mixed for SLS process, and the 3D printed MOFs devices with interconnective pore structure and porosity can be achieved. Combining the advantages of MOFs and SLS 3D printing can build new voids and open channels to increase the contact area, so that the fluids passing through the 3D printing devices can fully contact the MOFs fillers. However, this process may cause partial carbonization of the MOFs crystals, resulting in deterioration of its mechanical properties and accessibility of the active materials. Therefore, the post-printing-controlled layer-by-layer MOFs assembly on the surface , or directly integrating MOFs inside the 3D printed structure in one step can construct the complex 3D printed MOFs objects.

3D Printing Methods and Its Applications

Direct Ink Writing (DIW)

Various 3D printing approaches have been implemented to form structured MOFs materials, where extrusion-based 3D printing has been regarded as an attractive candidate for the shaping and consolidation of MOFs into monolith materials. DIW is a simple, flexible, and low-cost printing process in which materials (pastes or inks) are deposited stacktabily to build a final 3D structure (*27*). The key point of DIW is the controllabe rheology of the printing ink, that is, to prepare a slurry with ideal shear thinning and viscoelastic response properties (*28*). The shear thinning of the extrudable ink is to ensure continuous flow through a fine nozzle without clogging, while the superior viscoelastic response behavior allows rapid retention of shape and structure after extrusion. Therefore, the active material, dispersant and polymer binders are directly blended in the solvent to create stable printable inks.

For 3D printed MOFs composites, the utilization of DIW to produce and design MOF-based 3D monolithic materials with complex architectures, enhanced functionalities, and excellent mechanical properties, is still in the nascent stage. Most often, the DIW 3D printing technique is capable of programmatically manufacturing 3D MOFs devices by directly mixing nano-sized MOFs powder and polymetric binders or plasticizers into inks for further processing (*22*). However, this approach requires that MOFs ink must be optimized to produce a favorable rheology. Direct blending with non-porous matrix materials often reduces the effective MOF porosity, and causes the serious aggregation of MOFs particles and poor MOFs particle matrix connection, thereby limiting

their functioncal performance. Another strategy for preparing 3D printed MOFs bulk materials is in situ growth of MOFs coating onto the 3D printed supports, such as porous ceramics and hydrogel scaffold (*29*, *30*). However, most studies primarily focused on the growth of MOFs on the surface of the skeleton, resulting in the obvious limitations, including low MOFs loading efficiency and poor stability. There are two main methods for preparing 3D printed MOFs monolithic materials by in-situ growth: 1) Using DIW 3D printing to manufacture the macroscopic porous scaffolds with complex geometric shapes, and then depositing MOF crystals on the surface of porous scaffolds through step-by-step liquid-phase *in situ* growth to yield surface-loaded MOFs 3D monolithic materials; 2) Introducing MOF ligands into the precursor inks, followed by shaping the ink into desirable structures, and finally *in situ* grow MOFs through the coordination of organic ligands and metal ions to form the 3D printed bulk material with controllable mechanical properties and uniformly loaded MOFs.

In summary, the 3D printed MOFs bulk materials manufactured based on DIW 3D printing technology are mainly manifested in two aspects. The former is MOFs were served as fillers to be introduced into the polymer solution as custom-made inks, and then the robust 3D objects or monoliths with the required wall thickness, channel size, and density were precisely build. For instance, the MOF-74(Ni), UTSA-16(Co), HKUST-1, ZIF-8, Ni-BT, ZIF-7, UiO-66, CPL-1, and MIL-101 powders have been used to fabricate the 3D printed MOF monoliths with ultrahigh loadings. Moreover, these 3D printed MOF constructs were found suitable for various gas adsorption and separation, biobutanol and n-butanol recovery, and selective catalysis applications. The latter is the 3D printed MOF monoliths containing various supports can be formulated through post-treatment of the printed structures, where post-processing strategies include direct growth on the substrate or seeded growth strategies. These 3D printed supports mainly include porous ceramics and hydrogel scaffolds, while MOFs primarily involve HKUST-1, MIL-100(Fe), Tb-MOF and Eu-MOF, etc. In this part, we summarized the potential applications of 3D printed MOF structures and devices in catalysis, drug delivery, bone regeneration or construction, adsorptive separations and recovery, and energy storage. Therefore, the incorporation of functional MOFs into 3D printed monoliths results in these printed constructs with tunable properties by varying the printing parameters and MOFs structure and loading. Apart from changing properties, the fabrication of multiple complex parts possesses high shape fidelity, which are closely related with high precision and controllability.

DIW 3D Printing of Pure MOFs

Lim *et al*. directly printed colloidal gels (HKUST-1_{gel}) containing only ethanol and HKUST-1 nanoparticles into porous self-standing MOF monoliths that maintain the accessible porosity and surface area of the MOF after shaping (Figure 1a) (*26*). The HKUST-1_{gel} could be printed into any shape of close-packed monoliths, including square-shaped, circular pellet, and other suitable shaped solids (Figure 1b and 1c). The 3D printed HKUST-1 monoliths retained the exceptionally high crystallinity and porosity, high surface area and mesopore volume, and mechanical integrity of the overall structure (Figure 1d). In addition, the colloidal gel formed by the binder-free MOF nanoparticles could be used to build the freely-shaped MOF monoliths with extremely high MOF loadings, and HKUST-1_{gel} exhibited self-healing capabilities because it could hold the entire gel network together to form a high-profile mesh-like structure (Figure 1c). Because HKUST-1_{gel}, with no binders or additives, can be prepared in large quantities, this method provides a promising avenue toward MOFs shaping in functional applications. Afterwards, Lawson *et al*. used printing

and coordination of MOFs based on thermal sol-gel assembly to directly manufacture HKUST-1 monoliths, which was called as gel-print-grow (GPG) (Figure 1e) (*31*). After 3D printing of self-standing sol-gel with high concentration of precursors, the monoliths were heated to increase the ability of the overall precursor to converte into MOF, thereby producing enough crystallinity and maximizing the utilization of pores (Figure 1f).

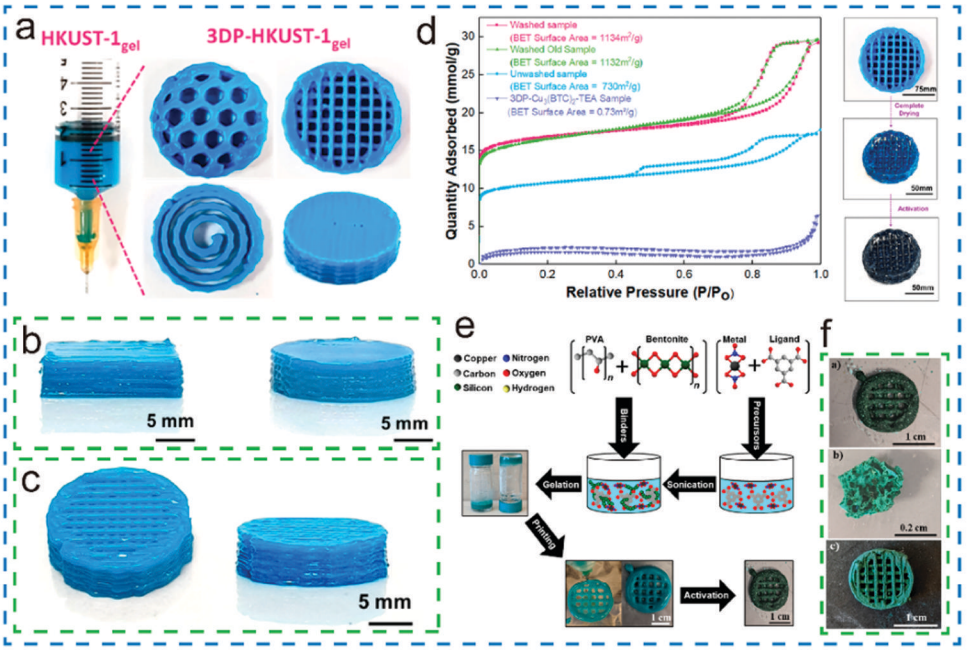

Figure 1. 3D printing of pure MOFs. (a) HKUST-1$_{gel}$ and 3D printed different HKUST-1 structures; (b) Side view of 3D-printed monoliths with square-shaped and circular pellet; (c) Top view of a 3D printed mesh-like monolith; (d) N_2 isotherms and photos of 3DP-HKUST-1$_{gel}$ at different processing stages. Reproduced with permission from ref. (26). Copyright 2019, American Chemical Society. (e) Schematic representation of the 3D printed HKUST-1 monolith prepared by novel GPG technique; (f) Activated HKUST-1 monolith after washing with acetone at 120 °C, cross-sectional view of the inner wall, and directly printed HKUST-1 monolith. Reproduced with permission from ref. (31). Copyright 2020, American Chemical Society.

DIW 3D Printed MOFs Porous Scaffolds

Pei *et al*. fabricated the biocompatible 3D mesoporous bioactive glass/MOF (MBG/MOF) scaffolds with well-controlled inner structure and pore morphology through 3D printing, and used it to deliver antitubercular drugs (*32*). The introduction of small particle size Fe-based MOFs into the MBG scaffolds is beneficial to control the drug delivery rate, enhance the mechanical properties, and adjust the pH microenvironment around the scaffolds. Hence, the MBG/MOF scaffolds possess potential in the therapy of osteoarticular tuberculosis. Dang *et al*. successfully prepared a new type of Cu-TCPP nanosheets interface-structured β-tricalcium phosphate (TCP) scaffold (Cu-TCPP-TCP) through combining MOFs materials with 3D printed porous bio-scaffolds (33). Owing to the outstanding photothermal performance of Cu-TCPP nanosheets, the Cu-TCPP-TCP scaffold can simultaneously ablate bone tumor tissues *in vivo* and kill the osteosarcoma cells *in vitro* under near-infrared (NIR) light. And based on the bone-forming bioactivity of TCP scaffolds, the biologically

active Ca^{2+} and PO_4^{3-} ions could be released, and finally the Cu-TCPP-TCP composite scaffold could also effectively promote the bone repair. Therefore, the 3D printing of MOFs nanosheets-structured scaffolds opens a new horizon to fabricate multifunctional biomaterials for tumor treatment and bone construction in tissue engineering.

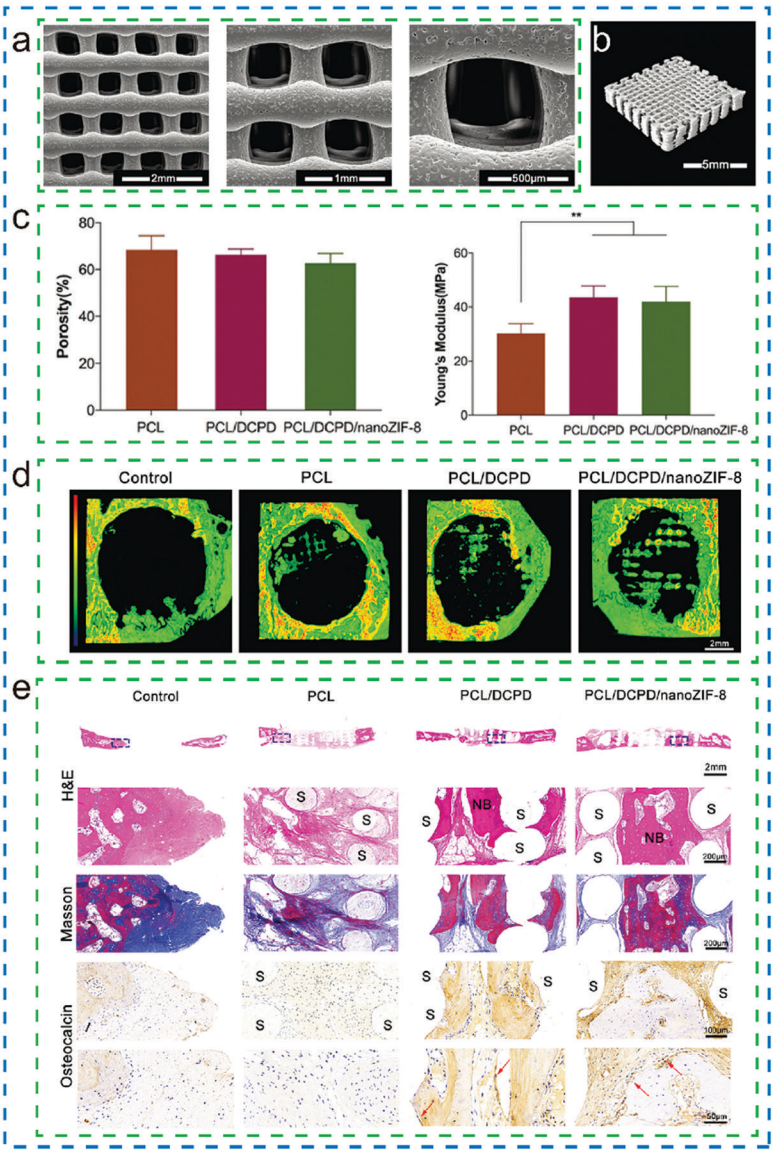

Figure 2. (a) SEM images of 3D printed PCL/DCPD/nanoZIF-8 porous scaffolds; (b) Micro-CT image of the PCL/DCPD/nanoZIF-8 scaffolds; (c) The porosity and Young's modulus of 3D printed porous scaffolds; (d) The 3D reconstruction images of the control group and 3D printed porous scaffolds; (e) Histological and immunohistochemical analysis of new bone formation conducted on decalcified samples; NB and S represent new bone and scaffold, respectively. Adapted with permission from ref. (34)*. Copyright 2020, The Royal Society of Chemistry.*

Zhong *et al*. homogeneously blended dicalcium phosphate dihydrate (DCPD) and nano ZIF-8 into melting polycaprolactone (PCL) to fabricate nanoZIF-8 modified 3D printed porous scaffolds (PCL/DCPD/nanoZIF-8) *via* extrusion-based 3D printing (*34*). Furthermore, the 3D printed porous scaffolds possessed a hierarchically porous structure (Figure 2a and 2b), in which the interconnected macropores increased the specific surface area for cell adhesion, and the sidewall pore structure facilitated the repairation of bone defects. Moreover, the porous scaffolds possessed high porosity and good mechanical properties (Figure 2c). The 3D printed PCL/DCPD/nanoZIF-8 porous scaffolds with biomimetic structure facilitated the regeneration of bone tissue *in vivo*, improved the healing of calvarial defect, and enhanced the proliferation activity of bone mesenchymal stem cells (BMSCs) (Figure 2d and 2e). These results show the effectiveness of nanoZIF-8 incorporation in 3D printed scaffolds to facilitate cell adhesion and proliferation in the treatment of bone tissue engineering.

DIW 3D Printed MOFs Hydrogel

Pei *et al*. blended Cu-BTC nanoparticles, sodium alginate (SA) and gelatin (GE) to prepare 3D printable ink, and crosslinked with $CaCl_2$ solution to fabricate 3D printed Cu-BTC/CA-GE scaffolds for organic pollutant adsorption (*35*). The as-obtained adsorbents with various well-defined patterns, such as square, hexagon, and circle, have been used to adsorb different organic dyes. The 3D printed MOFs adsorbent can also be easily regenerated without performance loss. Furthermore, the 3D printed MOFs adsorbents possessed the inherent microporous of MOF and the meso/microporous of 3D biocompatible polymers, which is beneficial to improve its adsorption performance.

Liu *et al*. created stretchable and tough 3D printing HKUST-1 hydrogel with tunable mechanical properties through DIW 3D printing, UV curing, ionic cross-linking, and *in situ* MOF growth (Figure 3a) (*30*). Moreover, by using a double network (DN) hydrogel precursor composed of acrylamide, alginate and MOF ligands as a 3D printable porous substrate, 3D printed MOF-hydrogel composites had high MOF particle dispersity, uniform macroscopic porous structure and high pore accessibility in the DN hydrogel matrix. The 3D printed HKUST-1 hydrogel was able to constructe customizable 3D MOF hydrogel shapes, such as dumbbell, pyramid, and grid (Figure 3b).

Huang *et al*. controlled 3D assembly of luminescent lanthanide MOFs (LnMOFs) through DIW 3D printing and post-printing treatment, and used it to construct 3D assembled LnMOFs-based optical sensing platform (Figure 3c) (*36*). By immersing the 3D printed constructs composed of organic ligands in the lanthanide ion solution, the *in situ* growth of LnMOFs rapidly occured through coordination with the ligand and chelation with the alginate matrix. The bicomponent combination inks could be used to construct different structures from 2D patterns to 3D scaffolds in a layer-by-layer manner on various substrates (Figure 3d). And the 3D printed LnMOFs objects with customizable geometries possessed tunable fluorescence properties, and responded to small molecules such as acetone. More interestingly, the 3D printed LnMOFs architectures with multiple fluorescent colors were also fabricated, such as the extruded fiber (Figure 3e and 3f) and 3D printed flower-like structure (Figure 3g and 3h). Overall, the applications of luminescent MOFs can bespeak the multiscale architectures of functional materials with controlled assembly.

Sultan and others have fabricated two 3D printed porous scaffolds with excellent shape fidelity based on a 3D printable hybrid hydrogel ink containing MOFs (ZIF-8 and MIL-100(Fe)) and 2,2,6,6-tetramethylpiperidine-1-oxylradical-mediated oxidized cellulose nanofibers (TOCNF)

(37). The presence of carboxylic groups on TOCNF surfaces facilitated the coordination of metal cations (Zn^{2+} or Fe^{2+}) with TOCNFs, that is, TOCNFs served as a carrier phase for MOFs growth *in situ*. The 3D printed ZIF-8@TOCNF (CelloZIF8) scaffolds (Figure 4a) and MIL-100(Fe)@TOCNF (CelloMIL100) (Figure 4c) have been successfully applied to encapsulate guest molecules, such as curcumin (Cur) and methylene blue (MB). The 3D printed CelloZIF-8 scaffolds were denoted as CelloZIF8-Cur (Figure 4a and 4b) and CelloZIF8-MB after wrapping the drug molecules curcumin and methylene blue, respectively. As shown in Figure 4d, the 3D printed CelloZIF8-Cur and CelloZIF8-MB scaffolds could release drug molecules under the pH stimuli-responsive, which is beneficial to extend the application of 3D printed CelloMOFs in the biomedical realms, such as the production of customized implants that release drugs to promote tissue healing and regeneration.

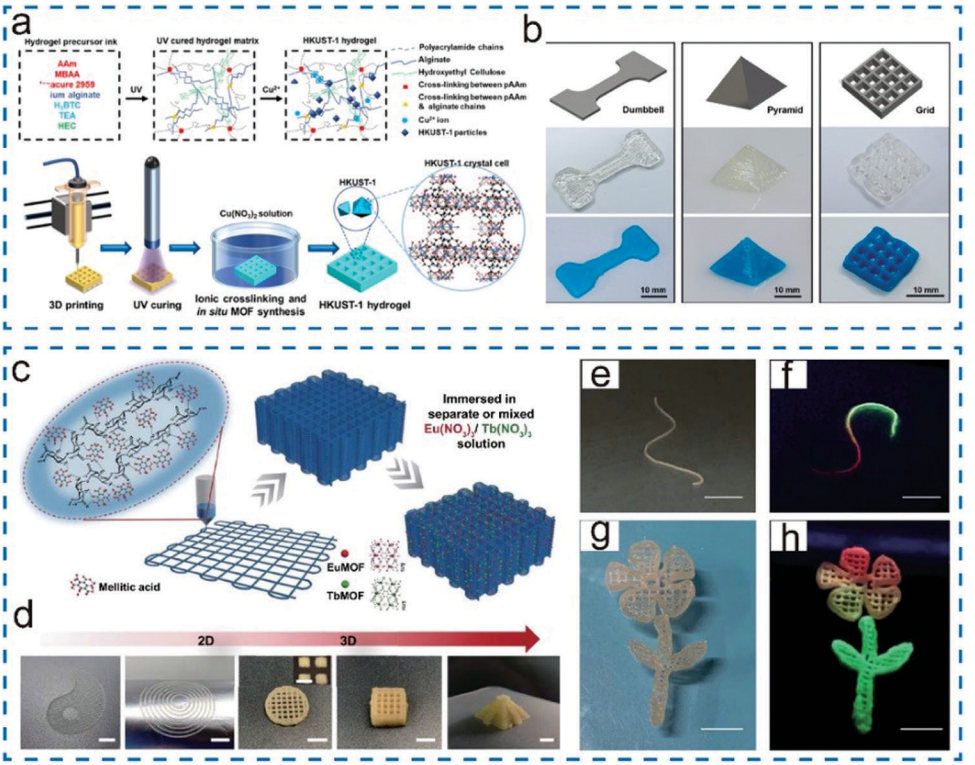

Figure 3. (a) Schematic diagram of the 3D printing process of HKUST-1 hydrogel; (b) 3D printed HKUST-1 hydrogel samples with dumbbell, pyramid and grid shapes. Reproduced with permission from ref. (30). *Copyright 2020, American Chemical Society. (c) Schematic diagram of the 3D printing LnMOFs objects; (d) Digital photos of 3D printed patterns and scaffolds with different structures (Scale bars: 5 mm); (e-h) Photographs of filament and 3D printed flower-like structure with tunable fluorescence (Scale bars: 1 cm). Reproduced with permission from ref.* (36). *Copyright 2021, Springer Nature.*

Hsieh *et al*. reported that bio-inks composed of ZIF-8 and polyurethane-gelatin (PUG) double network hydrogel were used to precisely fabricate customized tissues and organs (38). The ZIF-8 crystals as a network enhancer in PUG bio-ink could effectively tune the printability, stackability, thermoresponsiveness, mechanical and rheological properties of the PUG-ZIF-8 composite hydrogels. Furthermore, the PUG composite hydrogel containing ZIF-8 crystals could be utilized to fabricate hydrogel constructs with high water content and biological activity or compatibility, such as

blood vessel and ears of different sizes (Figure 4e-4i). In the future, the introduction of MOFs with reinforced effects into hydrogel inks can effectively tune the structural stability and modulus of 3D printing hydrogel constructs without sacrificing the water retention capacity of hydrogel inks, thus providing more possibilities for 3D bioprinting applications.

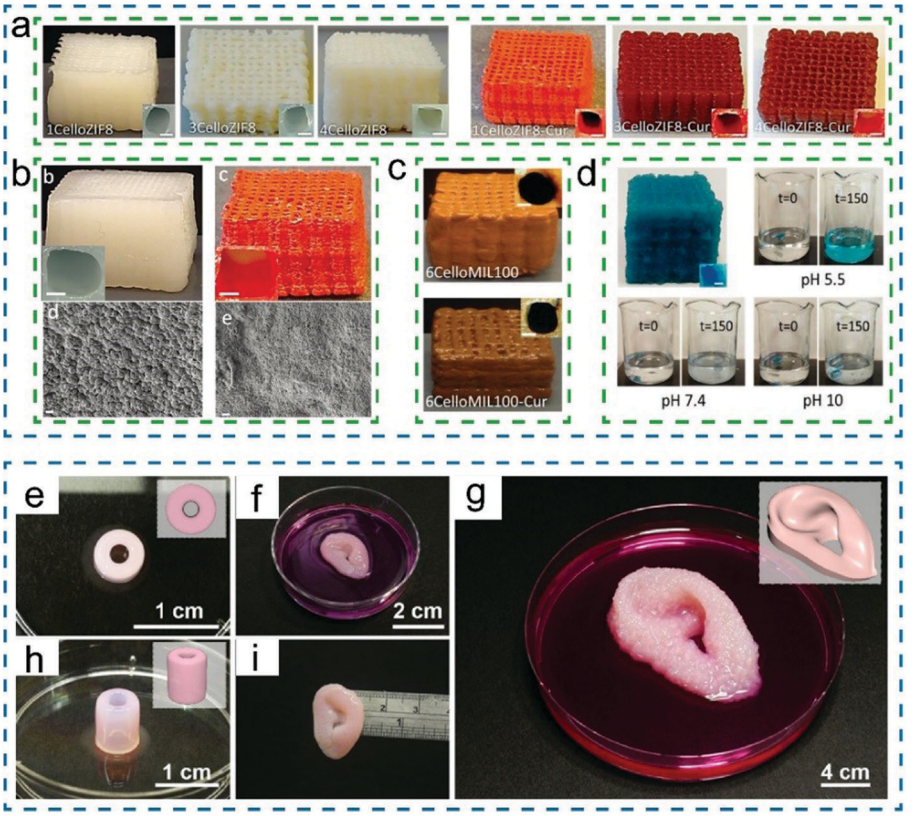

Figure 4. (a) Photos for 3D printed CelloZIF-8 scaffolds with and without curcumin. The insets show enlarged images of the pores in the printed scaffolds (Scale bars: 0.5 mm); (b) Photos of 3D printed CelloZIF8 and CelloZIF8-Cur scaffolds (Scale bars: 0.5 mm), and SEM images of the printed scaffolds (Scale bars: 1 μm); (c) Photos for 3D printed CelloMIL100 and CelloMIL100-Cur scaffolds (Scale bars: 0.5 mm); (d) Photos of 3D printed 4CelloZIF8-MB releasing MB at different pH values (Scale bars: 0.5 mm). Adapted with permission from ref. (37). *Copyright 2018, WILEY-VCH Verlag GmbH & Co. KGaA, Weinheim. (e, h) 3D printed blood vessel like constructs; (f, g ,i) Small- and large-size ear-shaped PUG hydrogel constructs. Reproduced with permission from ref.* (38). *Copyright 2021, American Chemical Society.*

DIW 3D Printed MOFs Structures for Adsorptive Separations

Thakkar *et al*. reported the utilization of 3D printing technique to fabricate nickel (MOF-74) and cobalt (UTSA-16) based MOFs into monolith structures, and evaluated their adsorptive performance for CO_2 capture in the air (22). The 3D printed self-standing MOF-74(Ni) and UTSA-16(Co) monoliths possessed high MOF loadings, and retained their physical and structural properties and mechanical integrity. Besides, the as-prepared self-standing 3D printed MOF monolithic had relatively good adsorption kinetics, showing it is suitable for various gas separation applications. Afterwards, Thakkar *et al*. developed two MOFs monolithic contactors for the

separation of ethane and ethylene through 3D printing, more specifically, Ni-BT and ZIF-7 were used as ethane-selective adsorbents (*39*). Furthermore, the 3D printed contactors with tailored geometry and structure possessed high porosity and excellent structural stability. And the 3D printed Ni-BT and ZIF-7 monoliths exhibited adsorption performance comparable to their powder counterparts, resulting in a high adsorption efficiency in separating ethane and ethylene.

In addition, Lawson *et al*. used pre- and post-impregnated two strategies to fabricate 3D printed amine-functionalized MIL-101 monoliths for dilute CO_2 adsorption (*40*). For pre-impregnation, the MIL-101 powder was impregnated with polyethylenimine (PEI) or tetraethylenepentamine (TEPA), and then shaped into MOF monoliths by 3D printing. Meanwhile, the postfunctionalization monoliths were manufactured by directly printing MIL-101 powders, and then impregnating the pristine MIL-101 monoliths with TEPA or PEI. However, the preimpregnated MOF monoliths will reduce the amine accessibility due to the dispersion of amine-functionalized MIL-101 into the monolith matrix, and the CO_2 adsorption rate was also limited by the diffusion of molecules into the monolith walls. Subsequently, Lawson *et al*. have produced polymer-MOF monoliths by 3D printing precursor seeds and subsequent secondary growth, in which 3D printed MOF-74 and HKUST-1 supports were used as seeds for secondary growth (*41*). The obtained HKUST-1@Torlon and MOF-74@Torlon monoliths possessed open channels, high MOFs loadings, and high surface area to volume ratio, which are beneficial to promote rapid mass transfer and improve adsorption capacity during the CO_2 adsorption processes.

Grande *et al*. reported a new non-aqueous cellulose-based ink composed of active UTSA-16, hydroxypropyl cellulose (HPC), isopropyl alcohol (IPA) and nanosized boehmite to fabricate 3D printed UTSA-16 monoliths, in which HPC polymer binder and boehmite additives were used to tailor the rheology of the ink (*42*). The printable ink containing UTSA-16 was printed into 3D periodic cylindrical structures, and the 3D printed UTSA-16 monoliths maintained the macro- and micro-structure after solidification (Figure 5a and 5b). Moreover, the 3D printed UTSA-16 monolith exhibited a considerably higher BET surface area, so it could be acted as a macro-porous adsorbent for CO_2 adsorption. Lefevere *et al*. reported the utilization of 3D printing fiber deposition strategy to fabricate ZIF-8 monolith adsorbents with open flow-through channels, in which methylcellulose and bentonite were used as organic and inorganic binders (Figure 5c) (*43*). Meanwhile, a thermal activation procedure was adopted to remove the organic binder from the structure, thereby achieving high adsorption capacity. The 3D printed ZIF-8 monolith could be used to separate the isopropanol-butanol-ethanol (IBE) model mixture under dynamic conditions, and the results showed that the ZIF-8 monolith possess high adsorption capacity and selectivity for *n*-butanol. Claessens *et al*. obtained two 3D printed ZIF-8 adsorbent monoliths with different fiber thickness, front channel size, and side channel size through layer-by-layer 3D printing, in which the printable ink containing the active ZIF-8 powder, binder bentonite, and plasticizer methylcellulose (Figure 5d and 5e) (*44*). The 3D printed ZIF-8 monoliths were effective for the separation of biobutanol from the acetone-*n*-butanol-ethanol (ABE) model mixtures, and the results indicated that the structured adsorbents with different channel size also have high adsorption capacity and selectivity for *n*-butanol (Figure 5f and 5g).

For the state-of-the-art MOF shaping, Dhainaut *et al*. manufactured a series of 3D MOF-based (HKUST-1, CPL-1, ZIF-8, and UiO-66-NH_2) solids with controlled morphologies and superior textural properties, where the shear-thinning inks consisted of MOFs powder, binder 2-hydroxyethyl cellulose and plasticizer poly (vinyl alcohol) (*45*). The as-prepared 3D MOF-based macroscale solids displayed permanent mechanical robustness, high porosity and specific surface area, which were

comparable to their powder counterparts. Furthermore, these robust macroscale structures were employed for methane gravimetric uptake (UiO-66-NH_2, ZIF-8, and HKUST-1) and ethane/ethylene separation (CPL-1), and the adsorption and separation performance are in line with their powder counterparts.

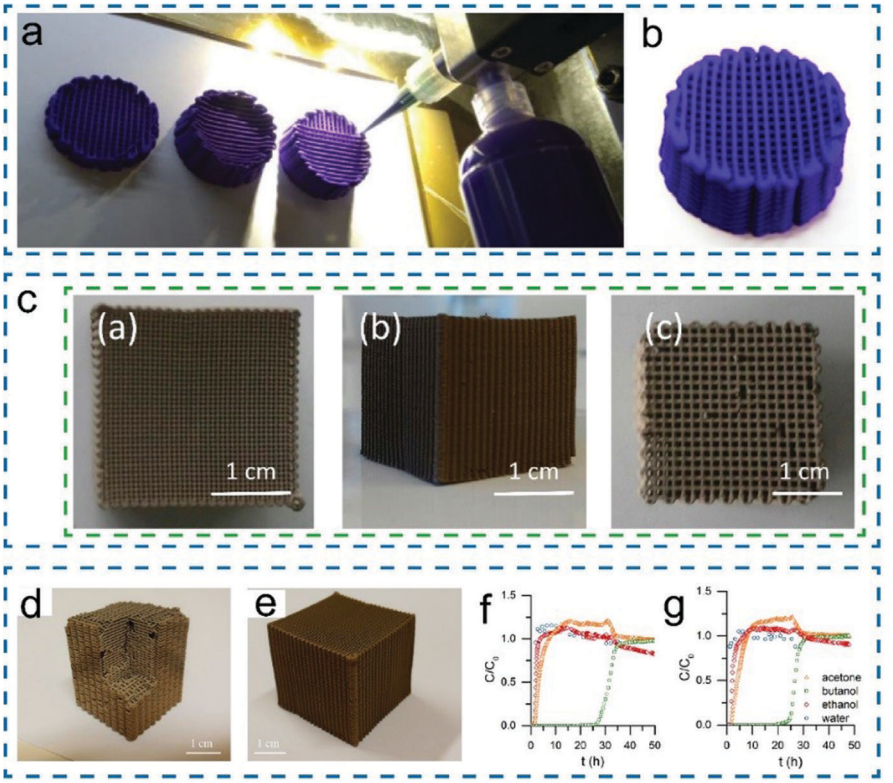

Figure 5. (a) 3D printed UTSA-16 monoliths with consistent periodic structures; (b) 3D printed UTSA-16 cylinder after drying (Diameter: 2.5 cm). Reproduced with permission from ref. (*26*). *Copyright 2020, Elsevier. (c) Photographs of the thermally activated 3D printed ZIF-8 monoliths with different fiber thickness (200 μm and 600 μm). Reproduced with permission from ref.* (*43*). *Copyright 2019, American Chemical Society. (d, e) Photographs of the 3D-printed ZIF-8 monoliths with different fiber thickness and channel size (250 μm and 600 μm); (f, g) Adsorption breakthrough profiles of vapor phase ABE mixtures on the 250 μm ZIF-8 monolith (f) and 600 μm ZIF-8 monolith (g). Reproduced with permission from ref.* (*44*). *Copyright 2020, American Chemical Society.*

DIW 3D Printed Ceramics Scaffolds and MOFs Coatings

Salazar-Aguilar *et al*. developed rectangular prismatic and cylindrical iron-based MOF/silicon carbide (SiC) scaffolds by DIW 3D printing of aqueous composite inks consisting of MOF-Fe/SiC powders, high molecular weight polyethylenimine (H-PEI), low molecular weight polyethylenimine (L-PEI), hydroxypropyl methylcellulose (MC), and ammonium polyacrilate (APA) (Figure 6a) (*46*). The microstructure of the 3D MOF-Fe/SiC cellular architectures showed that MOF-Fe seemed to have been fully integrated within the SiC ceramic structure (Figure 6b-d). The as-printed 3D MOF-Fe/SiC monoliths exhibited good mechanical strength, high robustness, and semiconductor-like

behavior (Figure 6e). Besides, the 3D periodic MOF-Fe/SiC lattices showed the remarkable catalytic performance and high selectivity in the hydroxylation reaction of phenol with hydrogen peroxide (Figure 6f and 6g).

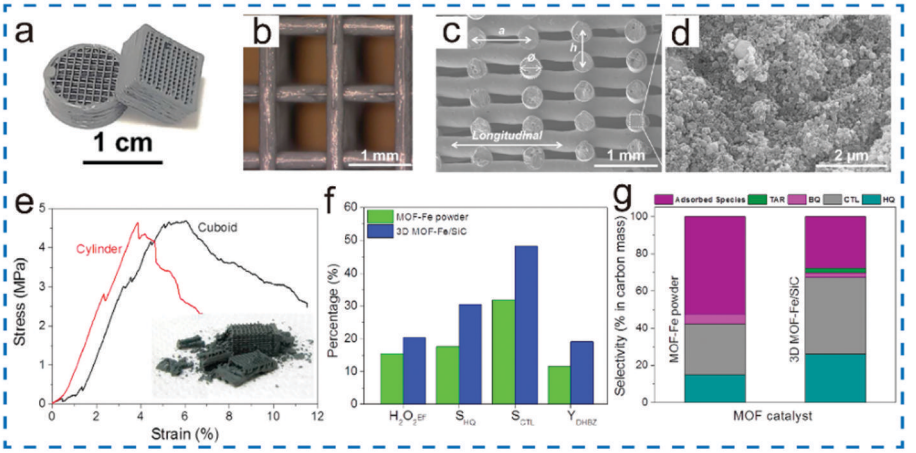

Figure 6. (a) Photos of as-printed MOF-Fe/SiC scaffolds with rectangular prismatic and cylindrical shapes; (b) Optical image showing a detail of the patterned structure in a cylinder; (c, d) FESEM micrograph and microstructure feature of MOF-Fe/SiC cylindrical scaffold after heat treatment; (e) Stress-strain curves for MOF-Fe/SiC prisms and cylinders. The inset shows the image of the prism collapsed after the compression test; (f, g) Catalytic performance and selectivity of 3D printed MOF-Fe/SiC in the hydroxylation of phenol. Adapted with permission from ref. (46). Copyright 2021, Elsevier.

Liu *et al*. reported the design of 3D printable hierarchical porous ceramics (3DP-HPC), which could be loaded with chemically active MIL-100(Fe) and HKUST-1 nanoparticles *in-situ* by facile hydrothermal treatment to endow the high catalytic performance (Figure 7a) (*29*). More importantly, the atalytic reactors, such as catalytic filter and agitating impeller, could be readily designed and fabricated by combining 3D-printing with *in-situ* MOFs growth (Figure 7b and 7c). The resultant atalytic reactors with desirable porous features exhibited outstanding catalytic degradation efficiency towards organic dyes, which was ascribed to its large surface area and numerous active sites in the interconnected porous networks.

DIW 3D Printed Structured MOF Catalysts

Young *et al*. used DIW 3D printing and UV-crosslinking 3D printable UiO-66 ink to manufacture 3D UiO-66 MOF structures, in which UiO-66 particles were dispersed in a mixture of commercially available acrylate monomer and photoinitiator (PI), and the chemically active UiO-66 particles were acted as the rheological modifier (*47*). After the organic binder was decomposed through selective thermal treatment, the as-obtained 3D UiO-66 composites with woodpile-type structures possessed mechanically stable and highly porous characteristics and, afterwards, the treated 3D printed UiO-66 monoliths had pore accessibility effective for the catalytic breakdown of a highly toxic nerve agent methyl-paraoxon. This work demonstrated that the incorporation of MOFs into 3D printable inks can significantly increase the stiffness of the monoliths, which contributes to the practical application of 3D printed MOFs and other functional materials in chemical conversion and catalysis.

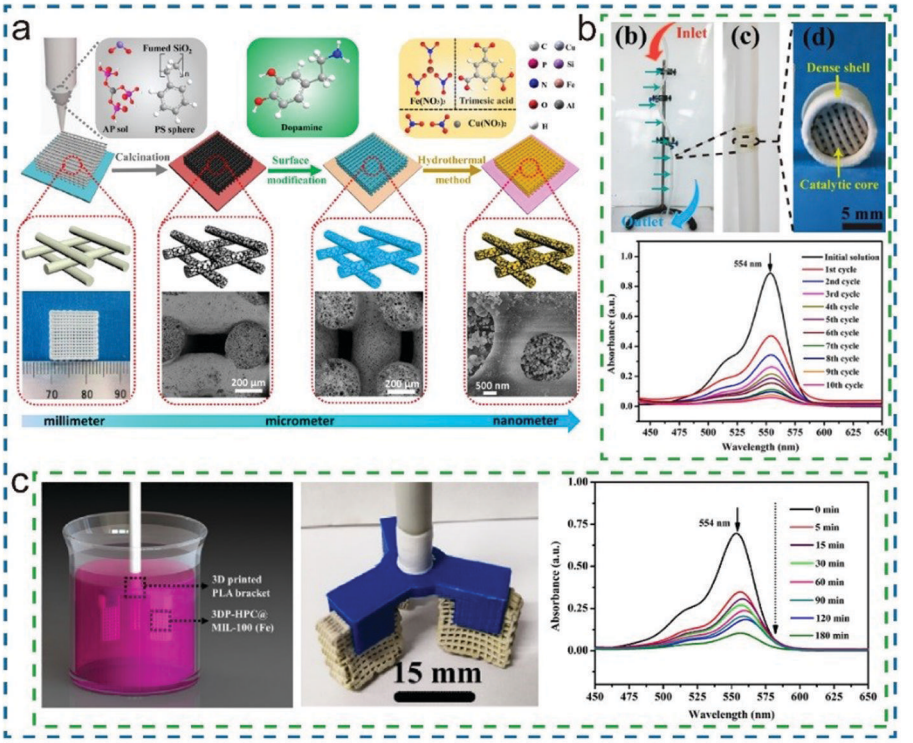

Figure 7. (a) Schematic diagram of well-ordered MOFs grown in situ on the 3D printed hierarchical porous ceramics; (b, c) 3D printed catalytic devices assembled with 3DP-HPC@MIL-100(Fe) filter (b) and the all-3D-printed impeller agitator with 3DP-HPC@ MIL-100(Fe), and its corresponding catalytic degradation performance (c). Adapted with permission from ref. (*29*)*. Copyright 2020, Elsevier.*

DIW 3D Printed MOF-Derived Hierarchically Porous Frameworks

Lyu *et al*. reported that a self-supporting printable Co-MOF-F127 ink composed of pre-synthesized Co-MOF crystals and Pluronic F127 to construct 3D printed Co-MOF frameworks (3DP-Co-MOF), and then thermal annealing to create a Co-MOF-derived hierarchically porous framework with good conductivity and mechanical stability (Figure 8a) (*48*). The novel self-standing, crack-free carbon framework could effectively serve as a porous conducting matrix (Figure 8b) to effectively deposit Li_2O_2 particles, and the presence of Co electrocatalysts could facilitate their decomposition. Moreover, the unique carbon framework owned abundant microscale pores formed between the Co-MOF-derived carbon flakes and the mesopores and micropores formed inside the flakes, and the Co nanoparticles embedded in nitrogen-doped mesoporous carbon flakes (3DP-NC-Co) after thermal annealing (Figure 8d-i). Therefore, this study demonstrates an alternative new pathway to integrate MOF-derived porous matrix into a self-standing porous architecture, which can significantly enhance the discharge capacity and increase the practical specific energy of aprotic Li-O_2 batteries (Figure 8c).

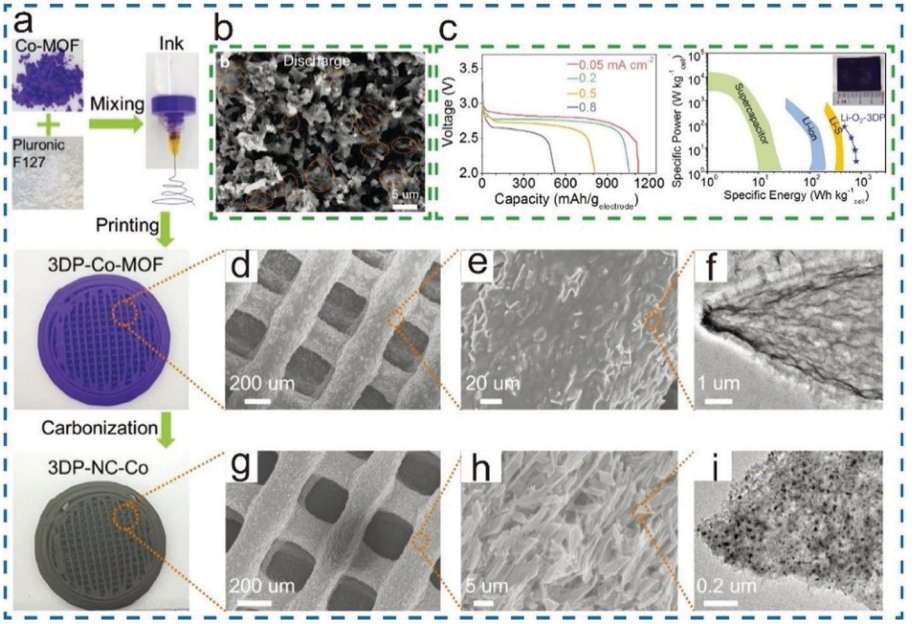

Figure 8. (a) The preparation diagram of 3DP Co-MOF-derived framework; (b) SEM image of pristine 3DP-NC-Co after discharge; (c) Rate capability (left) and Ragone plot (right) of 3DP-NC-Co; (d, e) SEM images of 3DP-Co-MOF; (g, h) SEM images of 3DP-NC-Co; (f, i) TEM images of 3DP-Co-MOF (f) and 3DP-NC-Co (i). Adapted with permission from ref. (*48*)*. Copyright 2018, WILEY-VCH Verlag GmbH & Co. KGaA, Weinheim.*

Fused Deposition Modeling (FDM)

Fused deposition modeling (FDM) is one of the most widely used 3D printing technologies because of its low-cost, technically simple, and ability to use commercially available filament materials, which relies on the layer-by-layer deposition of thermoplastic materials. The most common thermoplastic materials used for FDM include acrylonitrile butadiene styrene (ABS) (*49*), polylactic acid (PLA) (*49*), thermoplastic polyurethane (TPU) (*50*), polyamide (PA) (*51*) and polycarbonate (PC) (52), polyetherimide (PEI) (53), polyethylene (PE) (*54*), polypropylene (PP) (*55*) and polyvinyl alcohol (PVA) (*56*). In this process, the principle is that the thermoplastic filament is heated to its glass transition point, and then deposited layer by layer, cooled and hardened. For FDM 3D printing, moreover, the thermoplastic materials properties play a significant role in the mechanical properties and functionalities of 3D printed finished parts. Nevertheless, commercially available thermoplastic materials are generally limited by their functionality, which makes the prepared devices challenging in functional applications. In order to enhance the active chemical reactivity, functionality and mechanical properties of traditional filaments, the novel composite filaments were typically prepared by blending thermoplastics with the active materials or fillers such as graphene (*57*), carbon nanotubes (*58*), carbon fiber (*59*), metal oxide nanoparticles (*60*), and MOFs materials (*61*). Therefore, the integration of MOFs and FDM 3D printing can easily design and fabricate structured MOFs devices while maintaining their intrinsic functionality. And the 3D printed materials integrated with various MOFs structures can significantly improve the flexibility of the structured MOFs objects, while also can optimize any complex printed skeleton to deposit MOF coatings.

So far, there are three main strategies for the fabrication structured MOF composites or devices through a FDM 3D printing system: 1) The MOFs are immobilized on the 3D printed thermoplastic structure through layer-by-layer growth strategy (*62*). The as-obtained 3D printed thermoplastic polymer skeletons have the advantages of improving the stability of MOFs and controllable structural flexibility. The MOFs-coated 3D printing polymer composites not only avoid the separation process of MOFs powder, but also facilitate the recycling procedure. However, the disadvantage lies in the low MOFs loading and poor stability, and this layer-by-layer growth procedure is typically rather time-consuming. Moreover, the controlled MOFs layer-by-layer growth procedures after printing was limited by 3D printable materials that can absorb metals to initiate MOF growth; 2) The incorporation of metal oxides or MOFs metallic precursor into the thermoplastic polymers for filament extrusion, followed by post-printing and *in situ* conversion to MOF coatings (*63*). The principle is that the utilization of metal oxide precursor as a source of metal and converted it into MOFs *in situ* on the surface of 3D printed skeleton through coordination bond in the presence of the organic ligands. The preparation method possesses advantages of short time, high MOFs loading rate, and uniform growth of the MOFs crystal layer on the whole supports surface. Besides, the remaining metal oxide precursors in the 3D printed devices can be used to regenerate new MOFs coating, which contributes to improve the longer-term reusability and recyclability of 3D printed MOF-based devices. However, the main drawback is that the size and shape of the MOFs crystals depend on the selected 3D printing material, the amount of metal oxide or MOF metallic precursors, as well as the *in situ* MOFs growth circumstances; 3) MOFs are directly printed into 3D complex structure. Specifically, the pre-synthesized active material MOFs crystals were mixed with thermoplastic polymers to form MOF-thermoplastic polymer composite, and then extruded into melt-processable filaments for FDM 3D printing (*23*). In pioneering studies, some researchers have incorporated MOF-5, ZIF-8, HKUST-1, and UiO-66 materials into 3D printing thermoplastic polymers, forming MOFs-polymers composite filaments (*23*, *61*, *64*). This general strategy mainly addressed the processability shortcomings of MOFs and improves their structural stability and hydrolytic stability. However, a large part of matrix was composed of thermoplastic polymers, and few active MOFs are available, resulting in a low internal surface area.

In this section, we summarized the fabrication of 3D printed structured MOFs objects by introducing MOFs uniformly into the 3D structures through the FDM 3D printing, and discussed the applications in environmental remediation, gas storage and separation. Herein, MOFs crystals growth on 3D printed devices were achieved based on the direct printing of MOFs-polymers composite filaments and post-printing surface functionalization of the 3D printing frameworks, such as MOFs layer-by-layer growth and *in situ* conversion to MOFs coatings. The as-prepared 3D printed MOFs-polymers composites can not only retain the framework structure and functional characteristics of the MOFs powders, but also endow the material with new structures and performances, such as mechanical stability, flexible control of the structure, and the accessibility of the active sites of MOFs. Overall, the available potential multifunctional devices can be obtained by combining MOFs and FDM 3D printing, which is highly promising for the immobilization of powdered MOFs materials in practical applications.

MOF Layer-by-Layer Growth by FDM

Wang *et al*. successfully prepared a 3D printed acrylonitrile butadiene styrene (ABS) framework coated with porous Cu-BTC (Cu-BTC/ABS) by combining 3D printing and layer-by-layer in-situ growth strategy, which was used as an effective adsorbent for methylene blue (MB) removal (*62*).

After MB adsorption, the Cu-BTC/ABS composites could easily be recovered by washing with HCl solution and reused as a new skeleton for the secondary growth of MOFs, indicating that the 3D printed Cu-BTC/ABS composites had excellent recyclability and reusability. Afterwards, Shi *et al*. used biodegradable thermoplastic polylactic acid (PLA) to prepare 3D printed recyclable PLA skeletons with functional groups, followed by *in situ* growth of Cu-MOFs on its surface to fabricate a sustainable and environmentally friendly 3D printed Cu-MOFs/PLA film with different layers of Cu-MOFs coating (*65*). This process not only improves the stability of MOFs in water solution, but also facilitates the recovery process and practical application for MOFs adsorbents.

Pellejero *et al*. reported a 3D printed ABS filters functionalized with a thin layer of ZIF-8 material (ABS/ZIF-8) (Figure 9a), and the as-fabricated ABS/ZIF-8 filter offered excellent adsorption performance for toxic gas capture applications (*66*). The manufacturing strategy of ABS/ZIF-8 filters consisted 3D printed ABS polymer supports, atomic layer deposition (ALD) of metal oxide layers (ZnO), and secondary growth of MOFs. Moreover, ALD could form a uniform ultrathin ZnO layer on complex 3D structures (Figure 9b), where the ZnO layer was used as a reactive seeding for MOFs growth, resulting in uniform distribution of ZIF-8 crystals on the whole filter surface (Figure 9c). This kind of 3D printed filters functionalized with the active MOF layer exhibited excellent stability, so it was expected to be advantageously implemented in various environmental applications. Li *et al*. successfully fabricated the PLA/Fe-MOF hybrid supported photocatalysts by combining FDM 3D printing and plasma treatment, and the Fe-MOF coating was grafted permanently onto the surface of the 3D-printed fractal PLA substrates (*67*). The as-prepared PLA/Fe-MOF supported photocatalyst was used to degrade ciprofloxacin antibiotic in water under simulated sunlight irradiation.

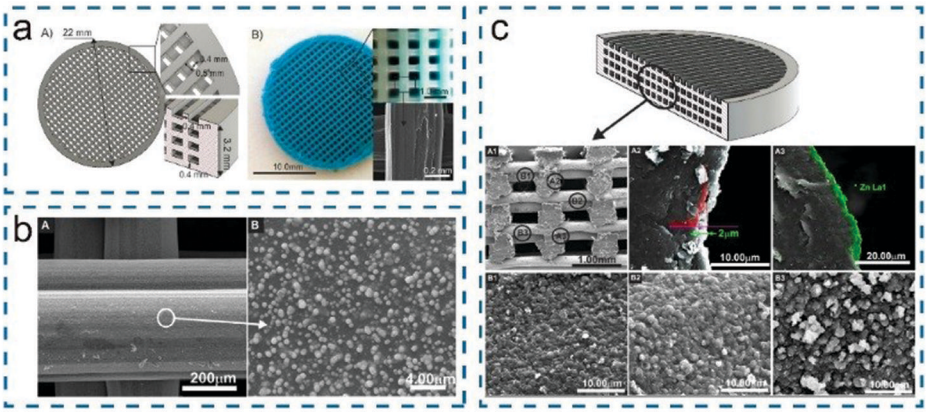

Figure 9. (a) CAD design of 3D printed ABS filter and printed pictures; (b) SEM images of ABS filter coated with ZnO; (c) Cross-sectional SEM images of different parts of the 3D printed ABS/ZIF-8 filter. Adapted with permission from ref. (*66*)*. Copyright 2020, Elsevier.*

FDM Printing of MOF Metallic Precursor/Polymer Composite Filaments and Post *In Situ* Conversion to MOF Coatings

Waheed *et al*. fabricated the 3D printable reactive composite filaments (ZnO-NP/ABS) by homogeneously blending nanoscopic MOF metal oxide precursor and thermoplastic ABS polymer (*68*). After 3D printing of ZnO-NP/ABS filament, in the presence of the organic ligand 2-methylimidazole, the ZIF-8 crystals were grown *in situ* on the 3D printed devices to fabricate the 3D printed ZIF-8@ZnO-NP/ABS devices (Figure 10a). The resultant 3D printed ZIF-8@ZnO-NP/

ABS devices were subsequently applied to remove organic pollutants from water (Figure 10b). This strategy can overcome the embedding of MOFs crystals into the 3D printed devices and expedite the growth of MOFs crystals on the skeleton surface. In addition, the unreacted metal oxide substrate is conducive to the regeneration of MOFs coatings on the 3D printed devices. Therefore, the post-3D printing *in situ* growth of MOFs will provide new opportunities for the design of multifunctional high-performance devices in environmental science, chemical separation or catalysis and other relevant applications. Liu *et al*. have successfully synthesized a novel Ca-MOF/ABS/TPU 3D framework by combining MOFs in-situ growth strategy and 3D printing (*63*). In this work, calcium silicate ($CaSiO_3$) was introduced into the melt ABS and thermoplastic polyurethane (TPU) blend to fabricate $CaSiO_3$/ABS/TPU filaments for FDM 3D printing, and then MOFs was directly loaded onto the 3D printed $CaSiO_3$/ABS/TPU skeleton surface etched by acetone. Before *in situ* growth of MOFs, the obtained 3D $CaSiO_3$/ABS/TPU skeleton was etched to expose more $CaSiO_3$ on the surface of framework, which was beneficial to provide more growth sites for MOFs. Overall, this work reports a novel strategy that combins MOFs and 3D printing to achieve powder immobilization, and the as-prepared Ca-MOF/ABS/TPU 3D scaffolds is alternative absorbent for the treatment of organic pollutants.

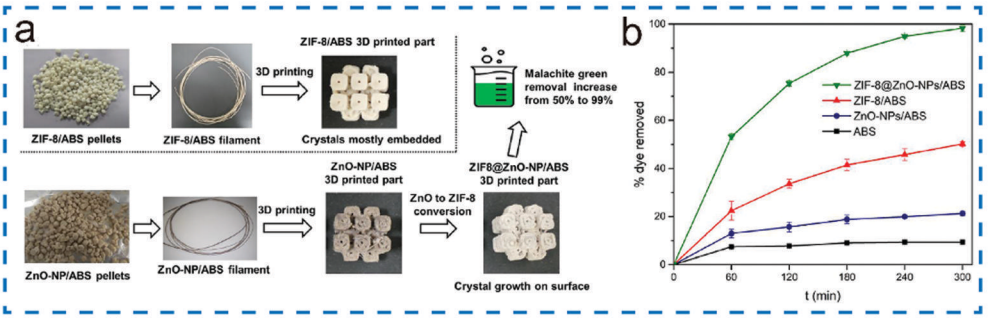

Figure 10. (a) Scheme for the preparation of ZIF-8/ABS and ZnO-NP/ABS composite filaments, and the preparation process of 3D printed ZIF-8@ZnO-NP/ABS devices; (b) MG removal performance of 3D printed ABS, ZIF-8/ABS, ZnO-NPs/ABS, and ZIF-8@ZnO-NPs/ABS devices. Adapted with permission from ref. (*68*)*. Copyright 2021, Elsevier.*

FDM 3D Printing of MOF-Thermoplastic Polymer Filaments and Objects

Bible *et al*. directly incorporated inorganic nanoparticles ZIF-8 and HKUST-1 into standard 3D printing thermoplastic polymer ABS to create 3D printing ABS-MOF composite filaments (*23*). These composite filaments were then printed into models with different geometries (Figure 11a). The 3D printed ABS-MOF composites (ABS-ZIF-8 or ABS-HKUST-1) had excellent processability and selective gas adsorption performance. For ABS-ZIF-8 or ABS-HKUST-1 composites, the crystalline MOF particles were evenly distributed within the amorphous polymer (Figure 11b-e). In addition, the ABS-MOF composites could be optimized to match the needs of these high-performance materials for emerging applications, including gas storage, gas filtration, catalysis, and real-time chemical sensing.

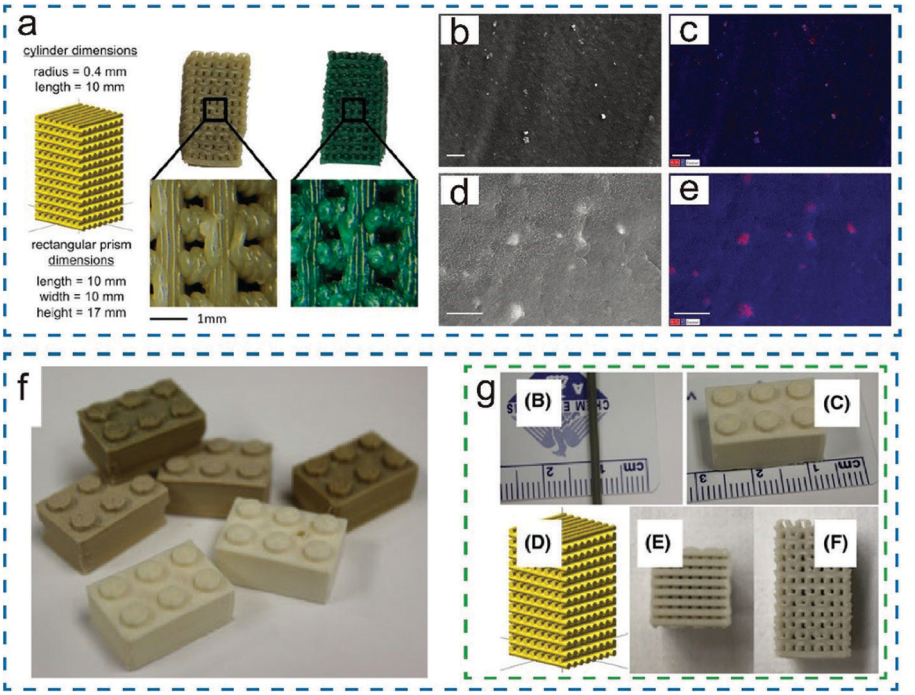

Figure 11. (a) The geometry and dimensions design of 3D printed MOF-ABS composites, as well as the images of full printed ABS-HKUST-1 and ABS-ZIF-8 composites and the magnification; (b, c) SEM images with EDS maps for ABS-ZIF-8; (d, e) SEM images with EDS maps for ABS-HKUST-1. Adapted with permission from ref. (*23*)*. Copyright 2018, Mary Ann Liebert, Inc. (f, g) ABS-MOF-5 filament and 3D printed objects with different MOF-5 content. Adapted with permission from ref.* (*64*)*. Copyright 2017, John Wiley & Sons, Ltd.*

Kreider *et al*. successfully prepared the 3D printable ABS-MOF-5 composite filaments, which could be printed into 3D devices for hydrogen storage (Figure 11f and 11g) (*64*). The 3D printed ABS-MOF-5 composite was a significant polymer-MOF material towards designing and 3D printing H_2 storage devices. However, the major shortcoming is that some MOF-5 was degraded due to the influence of ambient humidity during the process of preparing filaments. In addition, Evans *et al*. homogeneously incorporated MOFs nanoparticles (ZIF-8 or UiO-66) into TPU and PLA matrices to produce multifunctional MOF-thermoplastic polymer filaments for 3D printing feedstocks, and utilized to create macroscale 3D printed objects in well-defined and customizable forms (*61*). The 3D printed rigid PLA/MOF composites exhibited a large surface area and hierarchical porous internal network, whereas the flexible TPU/MOF composites did not have large voids and the micropores were blocked. These fabrication strategies can be extended to create 3D MOF structures or devices with complex internal structural features, and maintaining the valuable framework and chemical activity while also imparting new structural and functional properties in the printed objects.

Digital Light Processing (DLP)

Digital light processing (DLP) based 3D printing is a type of stereolithography, which involves localized photopolymerization of the photocurable precursor, layer over layer, to form complex 3D structures (*69*, *70*). Typical photocurable inks for DLP 3D printing are composed of photosensitive monomers or oligomers and a photo-initiator. Various printing parameters, including the exposure

time of each layer, UV light intensity, layer thickness, and the concentration and material formulations of photopolymer and photo-initiator, have been optimized to fabricate a high-resolution intricate structure. Moreover, DLP 3D printing has a high printing speed for liquid photocurable precursors that can integrate various functional elements including biomaterials and nanoparticles to manufacture multifunctional devices. MOFs as a promising class of porous functional materials, have been used as nanofillers to prepare functional 3D printed structures. In order to expose more MOF active sites within the printed objects, the combination of MOF particles and DLP 3D printing can not only improve the performance of MOFs, but also fabricate and design high-precision complex 3D objects with various functionalities.

The 3D MOFs structures based on DLP 3D printing can be achieved by the following three methods: 1) The utilization of photoactive resin composed of monomers or oligomers and photo-initiators to fabricate 3D printed devices or porous supports, and then MOFs coating was dip-coated or grown *in situ* layer-by-layer onto the 3D printed devices or supports (*71*). The obtained MOF-coated 3D printed devices generally retain the accessible porosity and surface aera of MOFs crystals, which is conducive to improving the activity of the 3D objects. However, the coating of the MOFs crystals on the 3D printed porous supports leads to poor long-term stability and durability, which is not beneficial to the practical applications. The procedures of this surface modification were time-consuming, and usually are limited to coating small-scale and accessible 3D printed structures with microporous materials; 2) The photocurable MOFs ink compositions containing monomers or oligomers, the crosslinker, MOFs particles, and photo-initiators directly produce complex and flexible 3D MOF-embedded polymeric structures (*72*). The 3D printed polymeric flexible objects contained MOFs exhibited excellent hydrolytic stability, and when MOFs is incorporated into the photocurable resins, it can also enhance the structural stability and mechanical properties of 3D printed functional devices. However, diametrically blending MOFs particles into photopolymerizable precursors as reaction mixtures might block the nanopores and adsorption sites of the MOFs particles, which may obstruct the intrinsic properties of the MOFs. The content of MOFs particles in the photocurable precursor is too high to form a stable dispersion for direct fabricating fine structures; 3) 3D free-standing MOFs objects composed predominantly of MOFs material are directly prepared during the printing process, and the 3D printed composite objects does not have any other binders or monomers (*73*). The key to this strategy is to find a coordination metal complexes or metal-containing-monomers (MCMs) as a monomeric building block, and this monomeric building block usually contains polymerizable functional groups and electron donating groups. The MCMs were utilized as the processing-ready MOF inks, which can polymerize to fabricate complicated free-standing objects during the printing process. According to the required application, the functionality of 3D MOF architectures can be tailored by the proper selection of metal ions and polymerizable ligands. This strategy enables MOFs powders to be manufactured into 3D printed complex objects for various fields and applications, including soft robotics, sensors and wearable electronic devices, as well as smart materials and bionic devices.

In this section, we summarized the 3D objects containing MOFs materials prepared by DLP 3D printing and their related applications. The utilization of photopolymerizable materials and functional MOFs that can form 3D printed MOFs devices with high stability and structural tunability, which is capable of rapid and efficient fabricating complex 3D objects, in the field of functional 3D printing. In particular, the dispersion of MOFs nanoparticles into 3D printable resins can construct 3D flexible and hydrolytically stable MOFs devices, such as flow reactors and 3D filters, which is widely compatible with a variety of photocurable materials and MOFs.

DLP 3D Printing Pure Free-Standing MOFs Objects

Halevi *et al*. successfully fabricated 3D free-standing complex objects composed solely of a coordination polymer (CP) through the utilization of DLP 3D printing, in which the photopolymerizable coordination nickel tetra-acrylamide as a monomer building block, while the printing process leads to the formation of the coordination polymers (*73*). To demonstrate this, 3D printed objects with various complex structures of Ni-acrylamide complexes were manufactured through this print-and-form strategy (Figure 12a-d). This work was expected to provide the new ideas for various applications that require complex architectures of stand-alone CPs, such as separation columns, reactive flow reactors, and reactor with built-in catalysts.

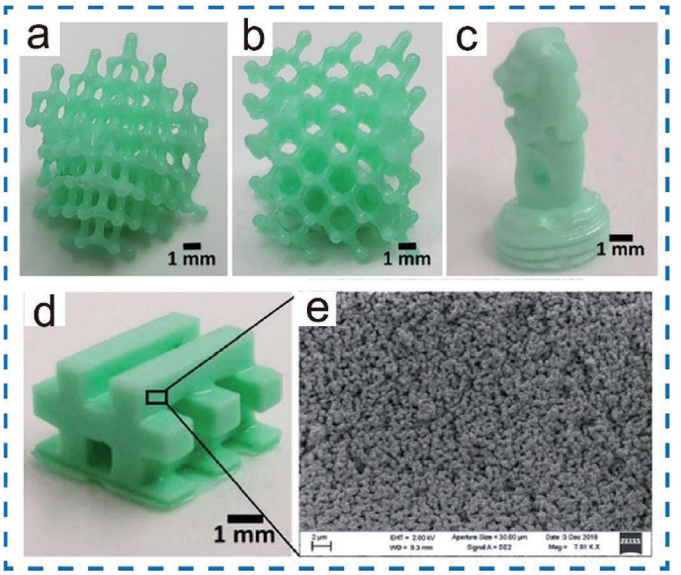

Figure 12. (a-d) Various complex 3D printed objects containing Ni-acrylamide complexes and SEM image of the cross-sections of the printed objects (e). Adapted with permission from ref. (*73*). *Copyright 2020, The Royal Society of Chemistry.*

3D Printed Skeletons with MOFs Porous Coatings

Figuerola *et al*. fabricated robust and intricate 3D printed devices (MOF-MMC) by incorporating ZIF-67/polymer mixed-matrix coating (MMC), where the 3D printed devices were fabricated by SLA 3D printing based on polyvinylidene fluoride/DMF (PVDF/DMF) mixtures (Figure 13a) (*74*). Besides 3D printed devices before and after coated with a MOF-MMC, various MOF-MMC 3D printed structures were also fabricated (Figure 13b-d). The developed MOF-MMC 3D printed devices have been used for the degradation of organic dyes in the formats of stirred-tank and flow-through column (Figure 13e and 13f), and the MOF-MMC 3D printed devices possessed excellent reusability and reproducibility. Therefore, this strategy would be desirable to incorporate micro/nanoparticulated materials on intricate 3D printed devices with a large size. Dong *et al*. successfully fabricated HKUST-1/SiO_2 composite material with specific structure by combining DLP 3D printing and step-by-step in-situ growth method (*71*). The SiO_2 ceramic substrate was constructed through 3D printing with photosensitive resin as the ceramic precursor polymer

combined with high-temperature pyrolysis, and HKUST-1 was coated on the surface of the SiO_2 ceramic skeleton as a recyclable catalyst, thus satisfying the concept of green chemistry.

Singh *et al*. developed a precision engineered 3D flow sensor (ZIF-8@OpdA@CSM) that integrates a catalytic enzyme (OpdA) onto a 3D printed catalytic static mixer (CSM) to maximize flow and interfacial interactions, where the crystalline ZIF-8 was not only used to protect and immobilize the enzymes, but the ZIF-8 pores offered access of the enzymes to the analytes and contaminants (75). The MOF@enzyme complex was coated onto the surface of 3D printed polymer static mixer, which is beneficial for increasing the flow rates and improving the efficiency of multiple run cycles. Therefore, ZIF-8@Enzyme@CSM system is suitable for continuous bioremediation and real-time monitoring applications in a range of fields, including the detection of organic toxins signals in water systems and the miniature sensors suitable for human health in personalized medicine.

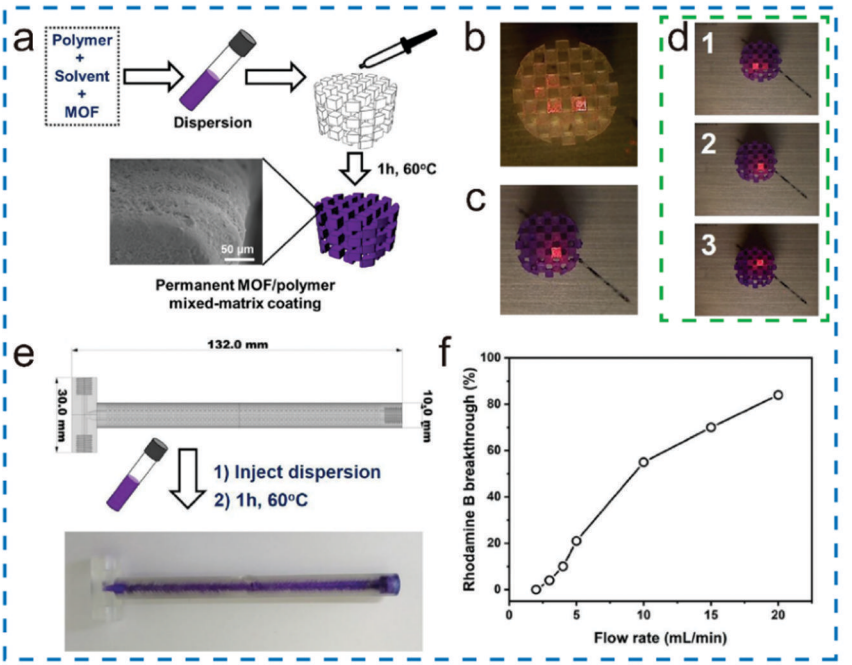

Figure 13. (a) Schematic representation of immobilizing MOF-MMC on 3D printed devices; (b, c) 3D printed devices before (b) and after (c) coating with a MOF-MMC; (d) Three different MOF-MMC 3D printed devices; (e) 3D printed columns with integrated interconnected cubes and MOF-MMC columns; (f) Effect of flow rate of 3D printed flow-through column on the degradation of organic dyes. Adapted with permission from ref. (74). *Copyright 2019, Elsevier.*

3D Printing Photocurable MOFs Inks and Objects

Chaudhari *et al*. have successfully developed the 3D printed objects capable of producing warm white light emission by combining fluorescent Guest@MOF compounds that emit yellow-light with a blue-emitting photosensitive polymer resin (72). Subsequently, various 3D printed luminescent composite objects that can convert UV into warm white light emission were designed (Figure 14a-f), which is beneficial for the construction of photonic sensors, optoelectronics, and energy-saving lighting devices. In addition, the emission chromaticity could be easily tuned by systematically changing the thickness of the 3D printed disc-shaped pellets (Figure 14g and 14h). This research demonstrates that the use of Dual-Guest@MOF and 3D printing that can achieve various geometric

shapes and designs has many advantages, such as permitting chromaticity adjustment and enhancing structural and photostability of the functional devices in the solid states 3D printed form.

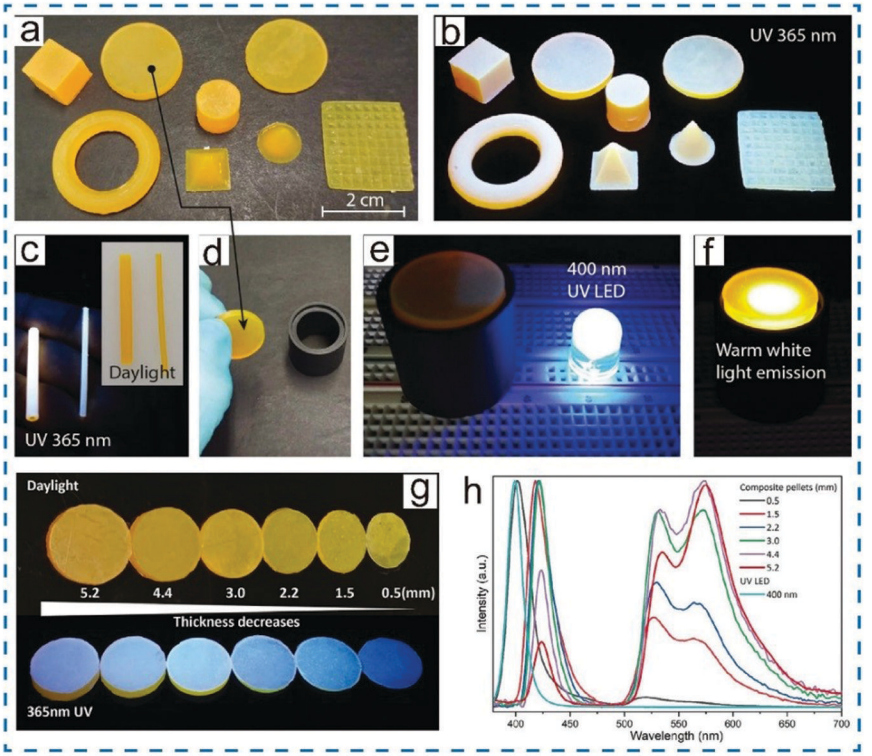

Figure 14. (a) Various shapes of 3D printed objects constructed from the fluorescent Guest@MOF compounds; (b, c) 3D printed objects that produce white light emission under UV irradiation; (d-f) A 3D printed disc-shaped pellet (d), mounted on a black cylindrical support (e), is used to convert 400 nm UV irradiation from the LED to produce warm white light emission (f); (g) Photographs and and their corresponding light-emitting objects of the 3D printed pellets with different thicknesses; (h) Tuneable pellet emission spectra as a function of pellet thickness. Adapted with permission from ref. (72). *Copyright 2020, WILEY-VCH Verlag GmbH & Co. KGaA, Weinheim.*

Maldonado *et al*. generated a series of new 3D printed thermochromic and solvatochromic composite objects (CP1@3D) based on the integration of multifunctional copper (II) 1D coordination polymer (CP1) with the stable polymerizable ink (Figure 15a), where CP1 was dispersed within dipropylene glycol diacrylate (SR-508) and ethoxylated trimethylolpropane triacrylate (SR-9035) monomers, and Irgacure819 and Irgacure184 were used as photoinitiators (*76*). The as-printed CP1@3D architecture could be used as an environmental humidity sensor to detect the relative humidity of the air, and it could also be used as a water sensor to detect a small amount of water in organic solvents (Figure 15b). These results indicated that the new 3D printed objects contained CP1 powder had the remarkable sensitivity to humidity in the air and low amounts of water in organic solvents, which may be due to the certain hygroscopic character and porosity of CP1. Therefore, the 3D printed CP1@3D objects with different architectures can be achieved from nonporous coordination polymer. Halevi *et al*. printed a flexible and hydrolytically stable MOF-based devices by combining Cu-BTC particles with photopolymerizable materials, where the MOF particles were dispersed in monomers SR-339 and SR-610 and photoinitiators Irgacure819 and

Irgacure184 (Figure 15c) (*24*). By this method, various complex and flexible MOF-embedded 3D polymeric structures (Cu-BTC@polymer) could be fabricated (Figure 15d), and the overall mechanical properties of 3D objects could be customized by selecting functional monomers (Figure 15d). This process enabled the fabrication of functional 3D MOF objects, such as matrices for columns and flow reactors, while retaining the adsorption capacity and activity of the printed MOFs and significantly improves its hydrolytic stability. Compared with the powder Cu-BTC, the 3D printed nets of Cu-BTC@polymer with a high macro surface area had high adsorption capacity for MB over short periods of time owing to exposing more Cu-BTC adsorption sites.

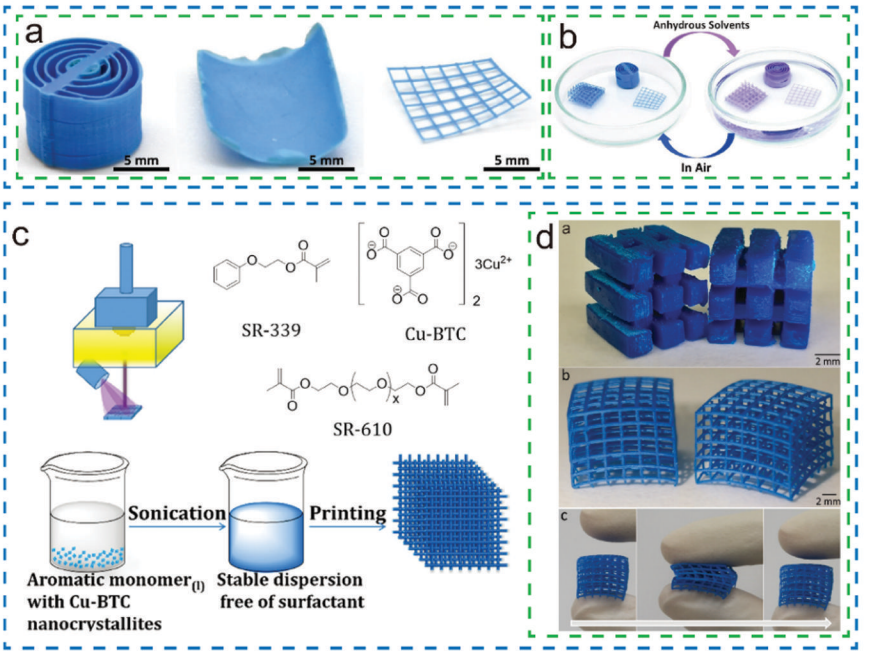

Figure 15. (a) 3D printed CP1@3D architectures with different shapes; (b) 3D printed CP1@3D objects with different architecture in air (blue color) and anhydrous solvents (violet color) at 25 °C. Adapted with permission from ref. (76). Copyright 2019, WILEY-VCH Verlag GmbH & Co. KGaA, Weinheim. (c) Schematic diagram of the photocurable components of 3D printing Cu-BTC@polymer and its forming the 3D object process; (d) 3D printed Cu-BTC@polymer with net structures, and flexibility display before, during, and after pressing. Adapted with permission from ref. (24). Copyright 2017, WILEY-VCH Verlag GmbH & Co. KGaA, Weinheim.

Selective Laser Sintering (SLS)

Selective laser sintering (SLS) is one of the most important industrial 3D printing processes, in which 3D solid functional parts with good details and surface finishes are constructed by the layer-by-layer sintering of polymer particles or powdered materials (*77*). These printable polymers or powdered materials mainly include thermoplastic polymers, ceramic powders and metal powders, etc., in which the most used thermoplastic polymers are polyamide 12 (PA12) and thermoplastic polyurethane (TPU) materials (*78*, *79*). Various other printable polymer materials with more flexible backbone and mechanical properties, such as polypropylene (PP) (*80*), polyethylene (PE) (*81*), and poly (ether ether ketone) (PEEK) (*82*), are also used to construct multifunctional 3D printed objects even further. The advantage of the SLS printing is that multiple 3D parts with high durability can

be fabricated without supporting structures, and no post-processing is required to further enhance the properties of the printed objects. With SLS 3D printing, the controllable multilayer structures with certain surface patterns can also be achieved, which is conducive to fine-tuning the mechanical properties, dimensional stability, and chemical functionalities of the objects. During the SLS process, a solid, porous, powder-bed-like object is created, which contains available voids when the polymer grains are partially sintered or melted together.

However, the incorporation of functional additives in the SLS 3D printed objects have been largely ignored. Furthermore, by blending SLS polymer powder and nanofillers to produce porous and solid objects conforms to this manufacturing trend. Besides, the introduction of nanomaterials, such as carbon black (*83*), metal oxide (*84*), and other inorganic nano fillers, lead to the reduction of mechanical behavior and flexural strength. In order to realize the practical applications of SLS processed products, it is still necessary to further improve the mechanical strength and versatility, such as wettability, adsorption and catalysis, and photo or thermo-responsive. MOFs composed of transition metal ions and linking ligands coordination have been identified as a promising new type of porous organic materials, and have attracted extensive applications in gas storage, adsorption, molecular separation, catalysis, luminescence and sensing, and molecular recognition. Thus, blending MOF nanofillers with polymer particles in the SLS process can produce parts with special structure, where polymer particles are used as printing matrix. Among the 3D printed parts obtained, the MOF fillers are attached to the surface of the sintered particles or embedded in the polymer matrix to form voids to provide open channels, and is therefore available for increase the contact area between the MOFs particles and the external environment to facilitate the flow of fluid through the 3D printed devices (*85*).

In this section, we focused on the laser sintering of MOFs composites to fabricate MOF-based functional parts for oil-water separation, wastewater treatment, and energy storage. Currently, there are two SLS 3D printing strategies used to print MOFs functional objects with desired mechanical properties and porous structures. The first one is that the printable composite powders were fabricated by mixing the pre-prepared MOFs nanofillers with an easily printable polymer matrix, which were then used to manufacture 3D MOF-based functional parts by SLS 3D printing, achieving the uniform embedding of MOFs nanofillers in the polymer matrix (*86*). The other is synthesizing nanofiller MOFs crystals in situ on the surface of the 3D printed polymer skeleton, which is beneficial to construct complex multiscale micro/nano structures (*87*). Therefore, various functional MOFs fillers and thermoplastic polymers were mixed for the SLS process, which can be applied to fabricate the practical devices with the MOFs embedded into the structure.

SLS 3D Printing Composite Powder Composed of MOFs Nanofillers and Polymer Particles

Lahtinen *et al*. incorporated HKUST-1 into the supporting polymer matrix Nylon-12 (N12) to fabricate highly porous 3D printed MOF/N12 disks (*85*). The 3D printed MOF/N12 disks were rigid and durable solids with high porosity, which can be used as flow-through filters and readily accessible for adsorption processes. Furthermore, the MOF crystals were firmly attached to the surface of the partially sintered polymer beads, and the functional components were not encapsulated by the N12 matrix. Therefore, by using SLS 3D printing, MOFs crystals can be converted into functional devices without destroying their structure or functional characteristics, which can be tuned to broaden the possible application range of MOFs. Li and colleagues applied SLS 3D printing technique to fabricate a series of single-layer and multi-layer MOF-PA12 mixed matrix films (MMFs) with various MOFs fillers (Figure 16a) (*86*). Specifically, the thermoplastic PA12 powder and five

types of MOFs crystals including NH_2-MIL-101(Al), MOF-801, HKUST-1, ZIF-67, and ZIF-8 crystals were blended as the printing materials (Figure 16b). These printed MOF-PA12 MMFs were highly porous, free-standing, and mechanically stable, resulting in high wetting efficiency, maximum adsorption capacity and rate, and good recyclability and durability (Figure 16c and 16d). The NH_2-MIL-101(Al)-PA12-10 MMF was hydrophilic in comparsion with the hydrophobic PA12 film and PA12 powder (Figure 16e). A three-layer MOF-PA12 MMF with a grid pattern was fabricated to confirm the feasibility of 3D MOF-polymer structure (Figure 16f). All the printed MOF-PA12 MMFs could be folded or shaped (Figure 16b), which demonstrates that the MOF-PA12 MMFs possess good recyclability and durability as an easy-to-collect adsorbent for water purification (Figure 16g).

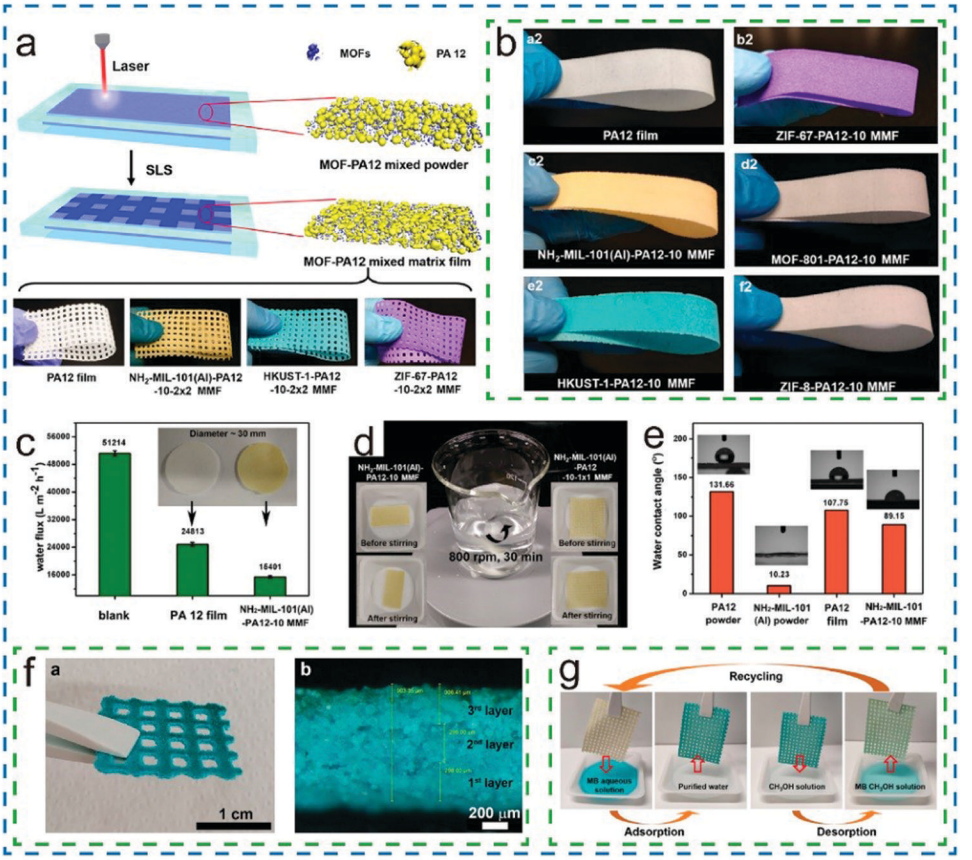

Figure 16. (a) Schematic procedure and photographs of 3D printed MOF-PA12 MMFs with grid patterns and various MOFs fillers; (b) Photographs of the printed PA12 film and MOF-PA12 MMFs; (c) Gravity-driven water flux and photographs of the PA12 film and NH_2-MIL-101(Al)-PA12-10 MMF; (d) Mechanical stability of 3D printed MOF-PA12 MMFs; (e) Water contact angles of 3D printed MOF-PA12 MMFs; (f) Photograph and cross-sectional micrograph of a three-layer HKUST-1-PA12 complex with grid pattern; (g) The adsorption and desorption process of NH_2-MIL-101(Al)-PA12-10-1×1 MMF. Reproduced with permission from ref. (85)*. Copyright 2019, American Chemical Society.*

Chen *et al*. successfully fabricated laser-sintered ZIF67-PA12 parts with porous structure by using the prepared feedstock material ZIF67-PA12 powders, where the *in situ* growth of nanofiller ZIF-67 crystals on the surface of PA12 polymer particles could expose the ZIF-67 nano-porous sites (25). Vaious ZIF67-PA12 parts with different structures were fabricated, such as solid, porous lattice structure, and mesh-like structures (Figure 17a-f). Moreover, the laser sintered porous lattice exhibited additional macropores and controlled cavities (Figure 17g and 17h). However, the as-printed ZIF-67-PA12 parts had poor mechanical performance compared to the plain PA12 (Figure 17i). Interestingly, the CO_2 absorption performance were significantly enhanced by designing the lattice structure of the parts and increasing the number of ZIF-67 active sites (Figure 17j). Therefore, the laser sintered functional parts with flexible design provide a new strategy for the wide applications of MOFs powder and MOF-polymer nanocomposites, such as energy storage and conversion.

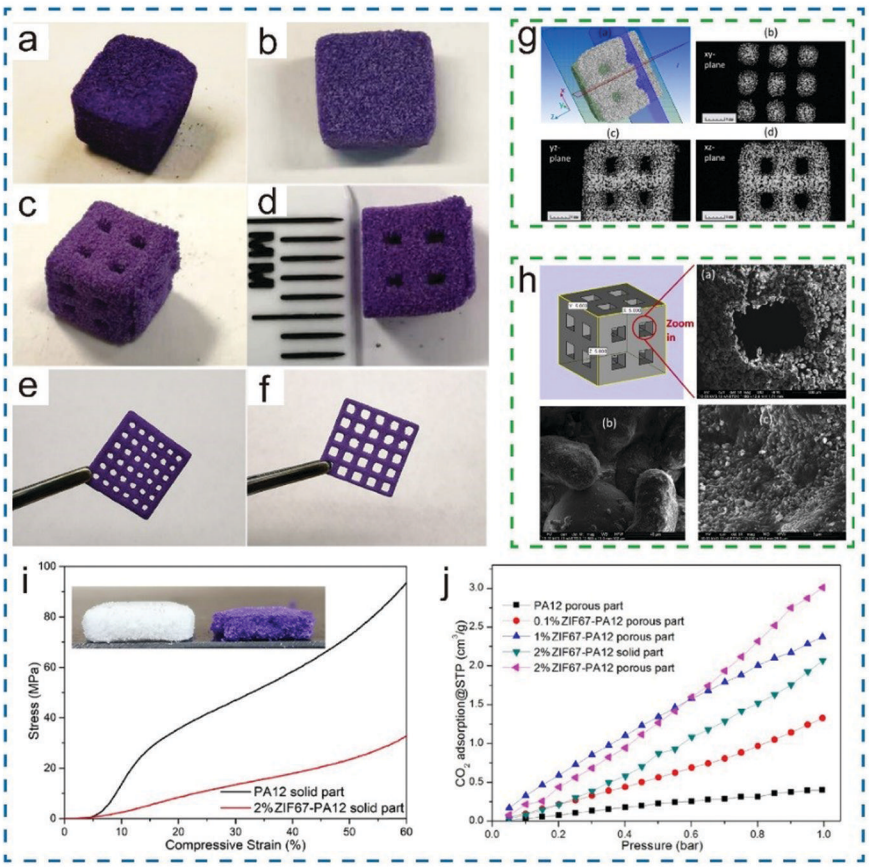

Figure 17. (a-f) The as-printed ZIF67-PA12 parts with different structures: (a, b) solid, (c, d) porous lattice structure, and (e-f) mesh-like structures; (g) Micro-CT 3D image of ZIF-67-PA12 porous part and its 2D image view in different planes; (h) SEM images of ZIF67-PA12 porous part; (i) Compressive curves of PA12 solid part and ZIF67-PA12 solid part, and its photos of after the compression test; (j) CO_2 adsorption capacities of PA12 porous part and ZIF67-PA12 solid and porous parts with different ZIF-67 content. Adapted with permission from ref. (25)*. Copyright 2021, Elsevier.*

In Situ Growth of Nanofiller MOFs Crystals on the Surface of SLS 3D Printed Polymer Skeletons

Yuan *et al*. successfully constructed a rough, porous and hierarchically micro/nanoscale structural surface on a rough SLS 3D printed PA membrane, which endowed the membrane with superwetting properties (*87*). In this study, the porous PA membrane was fabricated by SLS 3D printing, followed by a simple two-step deposition to grow a multiscale ZIF-Ls layers with leaf-crossed on the 3D printed porous PA membrane. The synthesized multiscale ZIF-Ls layers on the 3D printed membrane were coated with PDMS to produce a superhydrophobic 3D printed membrane (PDMS-MZIF15-PA) for oil-water separation. And the obtained PDMS-MZIF15-PA membrane possessed high oil rejection and super high oil flux. Therefore, through SLS 3D printing and designing 3D ZIF-Ls layer with leaf-crossed and multiscale structures, the complex multiscale micro/nano structured porous membranes can be produced.

Conclusions and Future Directions

Conclusion

In this perspective, we conclude the cutting-edge developments on 3D printed MOFs monoliths or devices, including their manufacturing approaches and potential applications in energy storage and conversion, catalysis, heavy metal ions and organic pollutants adsorption, bone regeneration, smart sensors, and light-emitting objects. The main technologies used to manufacture 3D printed MOFs monoliths or devices include DIW, FDM, DLP and SLS 3D printing. The prepared 3D MOF-based composites primarily have two types, the MOF-coated 3D printed objects and the all-integrated solid-state 3D structured MOFs parts. The 3D printed MOF-based monoliths possessed not only the characteristics of MOF materials, such as large surface area, high porosity and controllable components, but also the characteristics of supporting materials including high flexibility, strong mechanical properties and good biocompatibility. In addition, the categories, structures, performances and applications of 3D printed MOF-based monoliths were also discussed. In general, the applications of these tailor-made MOF-containing objects largely depend on the characteristics of the loaded MOFs and the supporting materials. For instance, in biomedical stents and drug delivery, the biocompatibility of the MOFs and the supporting material should be determined before practical use. Moreover, for the 3D printed MOF-based materials targeted to adsorbents, catalysts and membranes for water purification, the supporting materials must possess excellent mechanical properties to ensure the long-term stability and durability. The above-mentioned 3D structured MOFs composites possessed enhanced stability, accessibility, ease of handling and flexibility, and broaden the processability of MOFs powders in practical applications. Furthermore, the 3D printed MOF-based structures or devices also possessed high surface area, well-developed porosity and 3D printing-oriented interconnected porous framework, which is conductive to improving the accessibility and diffusion kinetics of large molecules. Despite these advantages, the 3D printed porous MOFs structures still have some drawbacks, including the cost of large-scale fabrication, the stability of MOFs in complex 3D structures, and the recyclability of MOFs components and supporting materials. It's believed that the complex 3D structures or functional objects with MOFs embedded or coated are an big step towards utilizing MOFs in functional devices. Finally, the future perspectives and insights associated with the manufacturing of 3D printed MOF-based composites in practical applications were discussed, including advanced multifunctional materials and structures.

Future Perspectives and Insights

3D Printing MOFs Composite Materials and Applications

(1) Future research will focus on the development of 3D printing MOFs hydrogel with network-like structures, which is beneficial to improve the performance of hydrogel matrix and promote the uniform distribution of MOF particles in the matrix. The 3D printed MOFs hydrogel can lead to the promising potential applications in biomedicine, flexible wearables and implantable sensors, and soft robotics due to their high pore accessibility, tunable mechanical properties, high water content and excellent biocompatibility. For instance, the addition of stimulus-responsive MOFs particles to 3D printed hydrogels can achieve on-demand drug delivery and control drug release efficiency under external stimulation, resulting in the 3D printed MOFs hydrogels with stimulus-responsive features.
(2) Future research on supporting materials such as MOF composite aerogels will also help to improve the practical applications of MOFs. Thus, various 3D printing techniques can be used in the future to manufacture the 3D printed MOFs aerogels with complex, free-form and interconnected architectures. Because 3D printed MOFs aerogels typically have the outstanding flexible, low density and excellent mechanical properties, they can be used as excellent support materials for loading active materials, such as drugs and catalysts.
(3) Another focus should be the 3D printed MOFs separation membrane for desalination and solar steam generation, catalysis, and water remediation. Generally, the synthesis of continuous and intergrown MOFs membrane on porous substrates through direct growth and secondary or seeded growth strategies requires heterogeneous nucleation, crystallization and crystal growth stages, which leads to grain boundary defects and intergranular cracks in the MOFs membrane. Comparing with the traditional MOFs polymer membranes, 3D printed MOFs membranes with various sizes, shapes and pores have obvious superiorities in terms of cost, flexibility, toughness and large-scale preparation, while retaining their high surface area to volume ratio, ordered pore structure and accessibility.
(4) Additionally, MOFs modified 3D printed porous ceramic scaffolds with micro- and macro-structures might be used as multifunctional biomaterials in tissue engineering treatment in future. For example, combining MOFs material with photothermal effects and 3D printed composite scaffolds can promote osteogenesis in bone tissue engineering.

Combination of 3D Printing and Other Manufacturing Processes

1. Combination of 3D Printing and MOFs Coating Technologies

The integration of MOFs active layer and 3D printed support layer can improve the performance of the 3D printed MOF structures. The porous supporting materials or substrates can make more MOFs active sites expose within the printed objects, where the MOFs coating is loaded or immobilized to the surface of the skeleton by means of spraying, spin-coating, and dip-coating. Moreover, the orderly arranged apertures and shapes of 3D printing are conducive to enhancing the transportation and flow of substances, while retaining the functionality and the hydrolytic stability of MOFs in the 3D printed frameworks.

2. Combination of 3D Printing and Electrospinning Technologies

The combination of 3D printing and electrospinning technologies can also create multifunctional layered structures that possess multi-scale porosity, where the electrospun mats are deposited onto the 3D printed layers to form the constructs with controlled properties. The 3D printed layer acts as macro-porous scaffolds to provide the robust support to maintain the shape integrity of the composite scaffolds. The electrospinning is instead used to fabricate ultrafine electrospun nanofiber network structure with tailorable pore sizes, high porosity and high surface area, which can effectively overcome the defects of large aperture and small porosity caused by single 3D printing technique. However, the currently developed electrospinning technology can only produce sub-micron diameter fibers and cannot achieve nano-scale characteristics. Therefore, the introduction of MOFs active materials into the electrospun layer can achieve biomimetic features and multiscale porosity, which is beneficial to construct biomimetic ion channels and promote the transportation of nutrients. More importantly, the fibrous mats contained MOFs can be attached uniformly on the macroscopic porous structure, which can effectively provide the bionic microenvironment to a certain extent. Therefore, the 3D printed MOFs composites prepared by integrating 3D printing and electrospinning process can find potential applications in the fields of tissue engineering scaffolds and water treatment membrane.

3. Integrated or Hybrid Manufacturing of Multiple 3D Printing Technologies

Hybrid fabrication strategies, like the combination of DLP printing or FDM printing and DIW printing, can be used to construct new hybrid multi-material functional structures and unique devices. With this hybrid 3D printing system, the advantages lie in on-demand fabrication, cost-effective production, and freedom of geometry design. Therefore, the introduction of MOFs nanoparticles into different printing systems can fabricate multicomponent and multi-functional devices with tunable properties, including strain sensors, catalysis and separation devices, and biomedical stents and drug delivery. For instance, using this hybrid 3D printing strategy, one type of MOFs can be introduced into two different 3D printing systems, or two MOFs with different attributes can be introduced into two 3D printing systems to achieve multi-material 3D printing structures and devices. Therefore, the hybrid 3D printing approach that integrates two or more 3D printing techniques provide a new and robust strategy for fabrication of complex multi-functional devices.

4. 4D Printing

Another exciting direction is the introducing stimulus-responsive MOFs into 3D printing systems to manufacture complex multifunctional devices, that is, 4D printed structures. Accordingly, with 4D printing, multi-functionality, shape transformations, and self-repair parts are possible. For example, 4D printing of smart MOFs porous membranes with tunable molecular separation, in which the pores of the membranes can be closed or opened under the external stimulus, allowing the permeation flux continuously adjusted for water-related applications. Besides, the surface wettability of the smart MOFs membranes can also be transformed into hydrophilic or hydrophobic under the external stimuli, such as temperature and environmental pH changes.

Acknowledgments

The work was financially supported by the National Natural Science Foundation of China (51775538 and 51935012), the Key Research Program of Frontier Sciences, CAS (QYZDY-SSW-JSC013), and the Western Light Project of Chinese Academy of Sciences.

References

1. Feng, L.; Wang, K.-Y.; Powell, J.; Zhou, H.-C. Controllable Synthesis of Metal-Organic Frameworks and Their Hierarchical Assemblies. *Matter* **2019**, 801–824.
2. Chen, L.; Xu, Q. Metal-Organic Framework Composites for Catalysis. *Matter* **2019**, *1*, 57–89.
3. Daglar, H.; Gulbalkan, H. C.; Avci, G.; Aksu, G. O.; Altundal, O. F.; Altintas, C.; Erucar, I.; Keskin, S. Effect of Metal–Organic Framework (MOF) Database Selection on the Assessment of Gas Storage and Separation Potentials of MOFs. *Angew. Chem. Int. Ed.* **2021**, *60*, 7,828–7837.
4. Kiadeh, S. Z. H.; Ghaee, A.; Bahi, A.; Ko, F. K. Electrospun pectin/modified copper-based metal-organic framework (MOF) nanofibers as a drug delivery system. *Int. J. Biol. Macromol.* **2021**, *173*, 351–365.
5. Li, J.; Wang, H.; Yuan, X.; Zhang, J.; Chew, J. W. Metal-organic framework membranes for wastewater treatment and water regeneration. *Coordin. Chem. Rev.* **2020**, *404*, 213116.
6. Koo, W.-T.; Jang, J.-S.; Kim, I.-D. Metal-Organic Frameworks for Chemiresistive Sensors. *Chem* **2019**, *5*, 1938–1963.
7. Zhu, L.; Zong, L.; Wu, X.; Li, M.; Wang, H.; You, J.; Li, C. Shapeable Fibrous Aerogels of Metal-Organic-Frameworks Templated with Nanocellulose for Rapid and Large-Capacity Adsorption. *ACS Nano* **2018**, *12*, 4462–4468.
8. Kalaj, M.; Denny, M. S., Jr.; Bentz, K. C.; Palomba, J. M.; Cohen, S. M. Nylon-MOF Composites through Postsynthetic Polymerization. *Angew. Chem.* **2019**, *58*, 2336–2340.
9. Zhu, M.-P.; Yang, J.-C. E.; Duan, X.; Zhang, D.-D.; Wang, S.; Yuan, B.; Fu, M.-L. Interfacial $CoAl_2O_4$ from ZIF-67@γ-Al_2O_3 pellets toward catalytic activation of peroxymonosulfate for metronidazole removal. *Chem. Eng. J.* **2020**, *397*, 125339.
10. Silva, M. P.; Ribeiro, A. M.; Silva, C. G.; Nogueira, I. B. R.; Cho, K.; Lee, U. H.; Faria, J. L.; Loureiro, J. L.; Chang, J.; Rodrigues, A. E.; Ferreira, A. MIL160(Al) MOF's potential in adsorptive water harvesting. *Adsorption* **2021**, *27*, 213–226.
11. Ban, Y.; Cao, N.; Yang, W. Metal-Organic Framework Membranes and Membrane Reactors: Versatile Separations and Intensified Processes. *Research* **2020**, *2020*, 1–13.
12. Cheng, Y.; Ying, Y.; Zhai, L.; Liu, G.; Dong, J.; Wang, Y.; Christopher, M. P.; Long, S.; Wang, Y.; Zhao, D. Mixed matrix membranes containing MOF@COF hybrid fillers for efficient CO_2/CH_4 separation. *J. Membr. Sci.* **2019**, *573*, 97–106.
13. Kalaj, M.; Bentz, K. C.; Ayala, S.; Palomba, J. M.; Barcus, K. S.; Katayama, Y.; Cohen, S. M. MOF-Polymer Hybrid Materials: From Simple Composites to Tailored Architectures. *Chem. Rev.* **2020**, *120*, 8267–8302.
14. Li, H.; Li, M.; Li, W.; Yang, Q.; Li, Y.; Gu, Z.; Song, Y. Three dimensional MOF-sponge for fast dynamic adsorption. *Phys. Chem. Chem. Phys.* **2017**, *19*, 5746–5752.

15. Li, X.; Liu, Y.; Wang, J.; Gascon, J.; Li, J.; Van der Bruggen, B. Metal–organic frameworks based membranes for liquid separation. *Chem. Soc. Rev.* **2017**, *46*, 7124–7144.
16. Parra-Cabrera, C.; Achille, C.; Kuhn, S.; Ameloot, R. 3D printing in chemical engineering and catalytic technology: structured catalysts, mixers and reactors. *Chem. Soc. Rev.* **2018**, *47*, 209–230.
17. Zhou, X.; Liu, C.-j. Three-dimensional Printing for Catalytic Applications: Current Status and Perspectives. *Adv. Funct. Mater.* **2017**, *27*, 1701134.
18. Zhang, D.; Xiao, J.; Guo, Q.; Yang, J. 3D-printed highly porous and reusable chitosan monoliths for Cu(II) removal. *J. Mater. Sci.* **2019**, *54*, 6728–6741.
19. Tijing, L. D.; Dizon, J. R. C.; Ibrahim, I.; Nisay, A. R. N.; Shon, H. K.; Advincula, R. C. 3D printing for membrane separation, desalination and water treatment. *Appl. Mater. Today* **2020**, *18*, 100486.
20. Low, Z.-X.; Chua, Y. T.; Ray, B. M.; Mattia, D.; Metcalfe, I. S.; Patterson, D. A. Perspective on 3D printing of separation membranes and comparison to related unconventional fabrication techniques. *J. Membr. Sci.* **2017**, *523*, 596–613.
21. Liu, T.; Sun, Y.; Jiang, B.; Guo, W.; Qin, W.; Xie, Y.; Zhao, B.; Zhao, L.; Liang, Z.; Jiang, L. Pd Nanoparticle-Decorated 3D-Printed Hierarchically Porous TiO_2 Scaffolds for the Efficient Reduction of a Highly Concentrated 4Nitrophenol Solution. *ACS Appl. Mater. Interfaces* **2020**, *12*, 28100–28109.
22. Thakkar, H.; Eastman, S.; Al-Naddaf, Q.; Rownaghi, A. A.; Rezaei, F. 3D-Printed Metal-Organic Framework Monoliths for Gas Adsorption Processes. *ACS Appl. Mater. Interfaces* **2017**, *9*, 35908–35916.
23. Bible, M.; Sefa, M.; Fedchak, J. A.; Scherschligt, J.; Natarajan, B.; Ahmed, Z.; Hartings, M. R. 3D-Printed Acrylonitrile Butadiene Styrene-Metal Organic Framework Composite Materials and Their Gas Storage Properties. *3D Print. Addi. Manuf.* **2018**, *5*, 63–72.
24. Halevi, O.; Tan, J. M. R.; Lee, P. S.; Magdassi, S. Hydrolytically Stable MOF in 3D-Printed Structures. *Adv. Sust. Syst.* **2018**, *2*, 1700150.
25. Chen, B.; Davies, R.; Chang, H.; Xia, Y.; Zhu, Y.; Ghita, O. In-situ synthesis of Metal Organic Frameworks (MOFs)-PA12 powders and their laser sintering into hierarchical porous lattice structures. *Addit. Manuf.* **2021**, *38*, 101774.
26. Lim, G. J. H.; Wu, Y.; Shah, B. B.; Koh, J. J.; Liu, C. K.; Zhao, D.; Cheetham, A. K.; Wang, J.; Ding, J. 3D-Printing of Pure Metal−Organic Framework Monoliths. *ACS Mater. Lett.* **2019**, *1*, 147–153.
27. Farahani, R. D.; Dube, M.; Therriault, D. Three-Dimensional Printing of Multifunctional Nanocomposites: Manufacturing Techniques and Applications. *Adv. Mater.* **2016**, *28*, 5794–821.
28. Minas, C.; Carnelli, D.; Tervoort, E.; Studart, A. R. 3D Printing of Emulsions and Foams into Hierarchical Porous Ceramics. *Adv. Mater.* **2016**, *28*, 9993–9999.
29. Liu, D.; Jiang, P.; Li, X.; Liu, J.; Zhou, L.; Wang, X.; Zhou, F. 3D printing of metal-organic frameworks decorated hierarchical porous ceramics for high-efficiency catalytic degradation. *Chem. Eng. J.* **2020**, *397*, 125392.
30. Liu, W.; Erol, O.; Gracias, D. H. 3D Printing of an In Situ Grown MOF Hydrogel with Tunable Mechanical Properties. *ACS Appl. Mater. Interfaces* **2020**, *12*, 33267–33275.

31. Lawson, S.; Alwakwak, A.-A.; Rownaghi, A. A.; Rezaei, F. Gel−Print−Grow: A New Way of 3D Printing Metal-Organic Frameworks. *ACS Appl. Mater. Interfaces* **2020**, *12*, 56108–56117.
32. Pei, P.; Tian, Z.; Zhu, Y. 3D printed mesoporous bioactive glass/metal-organic framework scaffolds with antitubercular drug delivery. *Micropor. Mesopor. Mater.* **2018**, *272*, 24–30.
33. Dang, W.; Ma, B.; Li, B.; Huan, Z.; Ma, N.; Zhu, H.; Chang, J.; Xiao, Y.; Wu, C. 3D printing of metal-organic framework nanosheets-structured scaffolds with tumor therapy and bone construction. *Biofabrication* **2020**, *12*, 025005.
34. Zhong, L.; Chen, J.; Ma, Z.; Feng, H.; Chen, S.; Cai, H.; Xue, Y.; Pei, X.; Wang, J.; Wan, Q. 3D printing of metal-organic framework incorporated porous scaffolds to promote osteogenic differentiation and bone regeneration. *Nanoscale* **2020**, *12*, 24437–24449.
35. Pei, R.; Fan, L.; Zhao, F.; Xiao, J.; Yang, Y.; Lai, A.; Zhou, S.-F.; Zhan, G. 3D-Printed metal-organic frameworks within biocompatible polymers as excellent adsorbents for organic dyes removal. *J. Hazard. Mater.* **2020**, *384*, 121418.
36. Huang, J.; Wu, P. Controlled Assembly of Luminescent Lanthanide-Organic Frameworks via Post-Treatment of 3D-Printed Objects. *Nano-Micro. Lett* **2021**, *13*, 15–28.
37. Sultan, S.; Abdelhamid, H. N.; Zou, X.; Mathew, A. P. CelloMOF: Nanocellulose Enabled 3D Printing of Metal-Organic Frameworks. *Adv. Funct. Mater.* **2019**, *29*, 1805372.
38. Hsieh, C.-T.; Ariga, K.; Shrestha, L. K.; Hsu, S.-h. Development of MOF Reinforcement for Structural Stability and Toughness Enhancement of Biodegradable Bioinks. *Biomacromolecules* **2021**, *22*, 1053–1064.
39. Thakkar, H.; Al-Naddaf, Q.; Legion, N.; Hovis, M.; Krishnamurthy, A.; Rownaghi, A. A.; Rezaei, F. Adsorption of Ethane and Ethylene over 3D-Printed Ethane-Selective Monoliths. *ACS Sustainable Chem. Eng.* **2018**, *6*, 15228–15237.
40. Lawson, S.; Griffin, C.; Rapp, K.; Rownaghi, A. A.; Rezaei, F. Amine-Functionalized MIL-101 Monoliths for CO_2 Removal from Enclosed Environments. *Energy Fuels* **2019**, *33*, 2399–2407.
41. Lawson, S.; Snarzyk, M.; Hanify, D.; Rownaghi, A. A.; Rezaei, F. Development of 3D-Printed Polymer-MOF Monoliths for CO_2 Adsorption. *Ind. Eng. Chem. Res.* **2020**, *59*, 7151–7160.
42. Grande, C. A.; Blom, R.; Middelkoop, V.; Matras, D.; Vamvakeros, A.; Jacques, S. D. M.; Beale, A. M.; Di Michiel, M.; Anne Andreassen, K.; Bouzga, A. M. Multiscale investigation of adsorption properties of novel 3D printed UTSA-16 structures. *Chem. Eng. J.* **2020**, *402*, 126166.
43. Lefevere, J.; Claessens, B.; Mullens, S.; Baron, G.; Cousin-Saint-Remi, J.; Denayer, J. F. M. 3D-Printed Zeolitic Imidazolate Framework Structures for Adsorptive Separations. *ACS Appl. Nano Mater.* **2019**, *2*, 4991–4999.
44. Claessens, B.; Dubois, N.; Lefevere, J.; Mullens, S.; Cousin-Saint-Remi, J.; Denayer, J. F. M. 3D-Printed ZIF8 Monoliths for Biobutanol Recovery. *Ind. Eng. Chem. Res.* **2020**, *59*, 8813–8824.
45. Dhainaut, J. r. m.; Bonneau, M. l.; Ueoka, R.; Kanamori, K.; Furukawa, S. Formulation of Metal−Organic Framework Inks for the 3D Printing of Robust Microporous Solids toward High-Pressure Gas Storage and Separation. *ACS Appl. Mater. Interfaces* **2020**, *12*, 10983–10992.

46. Salazar-Aguilar, A. D.; Quintanilla, A.; Vega-Díaz, S. M.; Casas, J. A.; Miranzo, P.; Osendi, M. I.; Belmonte, M. Iron-based metal-organic frameworks integrated into 3D printed ceramic architectures. *Open Ceramics.* **2021**, *5*, 100047.
47. Young, A. J.; Guillet-Nicolas, R. m.; Marshall, E. S.; Kleitz, F.; Goodhand, A. J.; Glanville, L. B. L.; Reithofer, M. R.; Chin, J. M. Direct ink writing of catalytically active UiO-66 polymer composites. *Chem. Commun.* **2019**, *55*, 2190–2193.
48. Lyu, Z.; Lim, G. J. H.; Guo, R.; Kou, Z.; Wang, T.; Guan, C.; Ding, J.; Chen, W.; Wang, J. 3D-Printed MOF-Derived Hierarchically Porous Frameworks for Practical High-Energy Density Li-O_2 Batteries. *Adv. Funct. Mater.* **2019**, *29*, 1806658.
49. Yang, H.; Ji, F.; Li, Z.; Tao, S. Preparation of Hydrophobic Surface on PLA and ABS by Fused Deposition Modeling. *Polymers* **2020**, *12*, 1539.
50. Leng, J.; Wu, J.; Zhang, J. Preparation of Thermoplastic Polyurethane Parts Reinforced with in Situ Polylactic Acid Microfibers during Fused Deposition Modeling: The Influences of Deposition-Induced Effects. *Ind. Eng. Chem. Res.* **2019**, *58*, 21476–21484.
51. Zhu, D.; Ren, Y.; Liao, G.; Jiang, S.; Liu, F.; Guo, J.; Xu, G. Thermal and mechanical properties of polyamide 12/graphene nanoplatelets nanocomposites and parts fabricated by fused deposition modeling. *J. Appl. Polym. Sci.* **2017**, *134*, 45332.
52. Salazar-Mart´ın, A. G.; P´erez, M. A.; Garc´iaGranada, A. e.-A.; Reyes, G.; Puigoriol-Forcada, J. M. A Study ofCreep in Polycarbonate Fused Deposition Modelling Parts. *Mater. Des.* **2018**, *141*, 414–425.
53. Li, M.; Jiang, J.; Hu, B.; Zhai, W. Fused deposition modeling of hierarchical porous polyetherimide assisted by an in-situ CO_2 foaming technology. *Compos. Sci. Technol.* **2020**, *200*, 108454.
54. Nabipour, M.; Akhoundi, B.; Saed, A. B. Manufacturing of polymer/metal composites by fused deposition modeling process with polyethylene. *J. Appl. Polym. Sci.* **2020**, *137*, 48717.
55. Wang, S.; He, H.; Peng, X.; Chen, H. Study on performances of graphite-filled polypropylene/polyamide 6 composites manufactured by fused deposition modeling. *J. Appl. Polym. Sci.* **2021**, *138*, e50751.
56. Wu, J.; Chen, N.; Wang, Q. Preparation of novel thermoplastic poly(vinyl alcohol) with improved processability for fused deposition modeling. *Polym. Adv. Technol.* **2018**, *29*, 1447–1455.
57. Dul, S.; Fambri, L.; Pegoretti, A. Fused deposition modeling with ABS-graphene nanocomposites. *Compos. Part A Appl. Sci. Manuf.* **2016**, *85*, 181–191.
58. Dul, S.; Fambri, L.; Pegoretti, A. Filaments Production and Fused Deposition Modelling of ABS/Carbon Nanotubes Composites. *Nanomaterials* **2018**, *8*, 49.
59. Ning, F.; Cong, W.; Hu, Y.; Wang, H. Additive manufacturing of carbon fiber-reinforced plastic composites using fused deposition modeling: Effects of process parameters on tensile properties. *J. Compos. Mater.* **2017**, *51*, 451–462.
60. Salea, A.; Prathumwan, R.; Junpha, J.; Subannajui, K. Metal oxide semiconductor 3D printing: preparation of copper(II) oxide by fused deposition modelling for multi-functional semiconducting applications. *J. Mater. Chem. C.* **2017**, *5*, 4614–4620.

61. Evans, K. A.; Kennedy, Z. C.; Arey, B. W.; Christ, J. F.; Schaef, H. T.; Nune, S. K.; Erikson, R. L. Chemically Active, Porous 3D-Printed Thermoplastic Composites. *ACS Appl. Mater. Interfaces.* **2018**, *10*, 15112–15121.
62. Wang, Z.; Wang, J.; Li, M.; Sun, K.; Liu, C. J. Three-dimensional printed acrylonitrile butadiene styrene framework coated with Cu-BTC metal-organic frameworks for the removal of methylene blue. *Sci. Rep.* **2014**, *4*, 5939.
63. Liu, Z.; Xia, X.; Li, W.; Xiao, L.; Sun, X.; Luo, F.; Chen, Q.; Qian, Q. In Situ Growth of Ca^{2+}-Based Metal–Organic Framework on $CaSiO_3$/ABS/TPU 3D Skeleton for Methylene Blue Removal. *Materials* **2020**, *13*, 4403.
64. Kreider, M. C.; Sefa, M.; Fedchak, J. A.; Scherschligt, J.; Bible, M.; Natarajan, B.; Klimov, N. N.; Miller, A. E.; Ahmed, Z.; Hartings, M. R. Toward 3D printed hydrogen storage materials made with ABS-MOF composites. *Polym. Adv. Technol.* **2018**, *29*, 867–873.
65. Shi, Z.; Xu, C.; Chen, F.; Wang, Y.; Li, L.; Meng, Q.; Zhang, R. Renewable metal–organic-frameworks-coated 3D printing film for removal of malachite green. *RSC Adv.* **2017**, *7*, 49947–49952.
66. Pellejero, I.; Almazán, F.; Lafuente, M.; Urbiztondo, M. A.; Drobek, M.; Bechelany, M.; Julbe, A.; Gandía, L. M. Functionalization of 3D printed ABS filters with MOF for toxic gas removal. *J. Ind. Eng. Chem.* **2020**, *89*, 194–203.
67. Li, K.; Miménand, Y. d. R. d.; Jin, X.; Yi, J.; Guo, J. Metal Oxide (ZnO and TiO_2) and Fe-Based Metal−OrganicFramework Nanoparticles on 3D-Printed Fractal Polymer Surfaces for Photocatalytic Degradation of Organic Pollutants. *ACS Appl. Nano Mater.* **2020**, *3*, 2830–2845.
68. Waheed, S.; Rodas, M.; Kaur, H.; Kilah, N. L.; Paull, B.; Maya, F. In-situ growth of metal-organic frameworks in a reactive 3D printable material. *Appl. Mater. Today* **2021**, *22*, 100930.
69. Fang, Z.; Shi, Y.; Zhang, Y.; Zhao, Q.; Wu, J. Reconfigurable Polymer Networks for Digital Light Processing 3D Printing. *ACS Appl. Mater. Interfaces* **2021**, *13*, 15584–15590.
70. Zhao, Z.; Tian, X.; Song, X. Engineering materials with light: recent progress in digital light processing based 3D printing. *J. Mater. Chem. C.* **2020**, *8*, 13896–13917.
71. Dong, J.; Li, P.; Guan, H.; Ge, C.; Bai, Y.; Zhao, Y.; Zhang, X. The synthesis of HKUST-1/SiO2 composite material based on 3D printing. *Inorg. Chem. Commun.* **2020**, *117*, 107975.
72. Chaudhari, A. K.; Tan, J. C. Dual-Guest Functionalized Zeolitic Imidazolate Framework-8 for 3D Printing White Light-Emitting Composites. *Adv. Optical Mater.* **2020**, *8*, 1901912.
73. Halevi, O.; Chen, J.; Thangavel, G.; Morris, S. A.; Uliel, T. B.; Tischler, Y. R.; Lee, P. S.; Magdassi, S. Synthesis through 3D printing: formation of 3D coordination polymers. *RSC Adv.* **2020**, *10*, 14812–14817.
74. Figuerola, A.; Medina, D. A. V.; Santos-Neto, A. J.; Cabello, C. P.; Cerdà, V.; Palomino, G. T.; Maya, F. Metal–organic framework mixed-matrix coatings on 3D printed devices. *Appl. Mater. Today* **2019**, *16*, 21–27.
75. Singh, R.; Souillard, G.; Chassat, L.; Gao, Y.; Mulet, X.; Doherty, C. M. Fabricating Bioactive 3D Metal–Organic Framework Devices. *Adv. Sust. Syst.* **2020**, *4*, 2000059.
76. Maldonado, N.; Vegas, V. G.; Halevi, O.; Martínez, J. I.; Lee, P. S.; Magdassi, S.; Wharmby, M. T.; Platero-Prats, A. E.; Moreno, C.; Zamora, F.; Amo-Ochoa, P. 3D Printing of a Thermo-

and Solvatochromic Composite Material Based on a Cu(II)–Thymine Coordination Polymer with Moisture Sensing Capabilities. *Adv. Funct. Mater.* **2019**, *29*, 1808424.
77. Singh, S.; Sharma, V. S.; Sachdeva, A. Progress in selective laser sintering using metallic powders: a review. *Mater. Sci. Technol.* **2016**, *32*, 760–772.
78. Aldahash, S. A. Optimum manufacturing parameters in selective laser sintering of PA12 with white cement additives. *Int. J. Adv. Manuf. Technol.* **2018**, *96*, 257–270.
79. Sun, S.; Gan, X.; Wang, Z.; Fu, D.; Pu, W.; Xia, H. Dynamic healable polyurethane for selective laser sintering. *Addit. Manuf.* **2020**, *33*, 101176.
80. Fang, L.; Wang, Y.; Xu, Y. Preparation of Polypropylene Powder by Dissolution-Precipitation Method for Selective Laser Sintering. *Adv. Polym. Technol.* **2019**, *2019*, 5803895.
81. Bai, J.; Zhang, B.; Song, J.; Bi, G.; Wang, P.; Wei, J. The effect of processing conditions on the mechanical properties of polyethylene produced by selective laser sintering. *Polym. Test.* **2016**, *52*, 89–93.
82. Wang, Y.; Shen, J.; Yan, M.; Tian, X. Poly ether ether ketone and its composite powder prepared by thermally induced phase separation for high temperature selective laser sintering. *Mater. Des.* **2021**, *201*, 109510.
83. Guaricela, J. L. B.; Ahrens, C. H.; Barra, G. M. d. O.; Merlini, C. Evaluation of poly(vinylidene fluoride)/carbon black composites, manufactured by selective laser sintering. *Polym. Compos.* **2021**, *2021*, 1–12.
84. Esmacher, O.; Hurst, M.; Regmi, G.; Velumani, S.; Castaneda, H.; Kuttolamadom, M. Selective laser sintering of metallic oxide powder mixtures for bi/tri-metallic-oxide formation. *Mater. Lett.* **2021**, *286*, 129215.
85. Lahtinen, E.; Precker, R. L. M.; Lahtinen, M.; Hey-Hawkins, E.; Haukka, M. Selective Laser Sintering of Metal-Organic Frameworks: Production of Highly Porous Filters by 3D Printing onto a Polymeric Matrix. *ChemPlusChem* **2019**, *84*, 222–225.
86. Li, R.; Yuan, S.; Zhang, W.; Zheng, H.; Zhu, W.; Li, B.; Zhou, M.; Law, A. W.-K.; Zhou, K. 3D Printing of Mixed Matrix Films Based on Metal-Organic Frameworks and Thermoplastic Polyamide 12 by Selective Laser Sintering for Water Applications. *ACS Appl. Mater. Interfaces* **2019**, *11*, 40564–40574.
87. Yuan, S.; Zhu, J.; Li, Y.; Zhao, Y.; Li, J.; Puyvelde, P. V.; Bruggen, B. V. d. Structure architecture of micro/nanoscale ZIF-L on a 3D printed membrane for a superhydrophobic and underwater superoleophobic surface. *J. Mater. Chem. A.* **2019**, *7*, 2723–2729.